Iron - based bulk amorphous alloys

R. Babilas*, R. Nowosielski

Division of Nanocrystalline and Functional Materials and Sustainable Pro-ecological Technologies, Institute of Engineering Materials and Biomaterials,
Silesian University of Technology, ul. Konarskiego 18a, 44-100 Gliwice, Poland
* Corresponding author: E-mail address: rafal.babilas@polsl.pl

ABSTRACT

Purpose: The paper presents a structure characterization, thermal and soft magnetic properties analysis of Fe-based bulk amorphous materials in as-cast state and after crystallization process. In addition, the paper gives some brief review about achieving, formation and structure of bulk metallic glasses as a special group of amorphous materials.

Design/methodology/approach: The studies were performed on $Fe_{72}B_{20}Si_4Nb_4$ metallic glass in form of ribbons and rods. The amorphous structure of tested samples was examined by X-ray diffraction (XRD), transmission electron microscopy (TEM) and scanning electron microscopy (SEM) methods. The thermal properties of the glassy samples were measured using differential thermal analysis (DTA) and differential scanning calorimetry (DSC). The magnetic properties contained initial and maximum magnetic permeability, coercive force and magnetic after-effects measurements were determined by the Maxwell-Wien bridge and VSM methods.

Findings: The X-ray diffraction and transmission electron microscopy investigations revealed that the studied as-cast bulk metallic glasses in form of ribbons and rods were amorphous. Two stage crystallization process was observed for studied bulk amorphous alloy. The differences of crystallization temperature between ribbons and rods with chosen thickness are probably caused by different amorphous structures as a result of the different cooling rates in casting process. The SEM images showed that studied fractures could be classified as mixed fractures with indicated two zones contained "river" and "smooth" areas. The changing of chosen soft magnetic properties (μ_r, B_s, H_c) obtained for samples with different thickness is a result of the non-homogenous amorphous structure of tested metallic glasses. The annealing process in temperature range from 373 to 773 K causes structural relaxation of tested amorphous materials, which leads to changes in their physical properties. The qualitative phase analysis from X-ray and TEM diffraction data enables the identification of a single phase of α-Fe for sample annealed at 823 K and a mixture of Fe_2B, Fe_3B and $Fe_{23}B6$ and α-Fe phases for samples annealed at temperature of 873 and 923 K.

Practical implications: The magnetic properties allow to classify the studied Fe-based glassy alloy for suitable material for electric and magnetic applications. These properties of could be improved by applying the appropriate conditions of heat treatment (crystallization process).

Originality/value: The applied investigation methods are suitable to determine the changes of structure, thermal and magnetic properties in function of sample thickness or annealing conditions.

Keywords: Amorphous materials; Bulk metallic glasses; Thermal and magnetic properties; Crystallization

Reference to this paper should be given in the following way:

R. Babilas, R. Nowosielski, Iron - based bulk amorphous alloys, Archives of Materials Science and Engineering 44/1 (2010) 5-27.

RESEARCH MONOGRAPH

1. Introduction

The definition of amorphous material is a general term which is refer to solid state with non-periodical atomic arrangement. The special feature of atomic structure of amorphous material in comparison with crystalline material is the non-long range arrangement of atoms. However, the atomic arrangements in atomic scale (distance of few diameters of atoms) is periodical [1].

The definition of amorphous structure is not clear. In general, it is obvious that amorphous material is material which has ordered region (crystallite) not higher than 1 nm. Based on the size of crystallite, materials could be classified on amorphous, nanocrystalline, microcrystalline and crystalline materials (Fig.1) [2].

The structure of crystalline materials could be easily determined by describing of unit cell in crystals. Characterization of amorphous structure is much more difficult because of broadening of diffraction patterns and lack of reflections during X-ray investigations [3].

Two-dimensional diagram of atoms network could be used to simple characterization of crystal, amorphous and gas structure. It is noticed that each atom in the amorphous material has three neighbours in similar distance, but in crystal that atomic distance is strictly equal [1].

The examinations of amorphous materials are also realized by many conventional methods like X-ray diffraction analysis, Mössbauer spectroscopy, neutron diffraction, transmission electron microscopy or computer aided modelling [1].

Information about atoms positions could be achieved by using radial distribution function (RDF). That method allows to obtain the general correlation of atomic arrangements, a number of the closest neighbours and an average atomic distance [4].

The radial distribution function is a probability of finding the atom in distance between r and $r+\delta r$ from centre of referring atom used as beginning of co-ordinate system. A comparison of radial distribution function for amorphous material with RDF of crystalline alloy may give some additional information of local structure [4].

The amorphous structure of materials could be described by two kinds of disorder [2]:
- topological,
- chemical.

The topological disorder is a result of dispersion of distances arrangement of atoms because of lack of repeatable geometric packing. The chemical disorder is a result of local environment of each atoms. In amorphous structure we could also determine the long range and close range arrangement of atoms [2].

Describing of amorphous structure could be also aided by modeling and simulation techniques. The modelling of amorphous structure is concentrated on model of liquid metal also known as Bernal's model - DRPMHS (Dense Random Packing Model of Hard Spheres). That model is built on dense random packing hard spheres [1].

Amorphous materials could be fabricated by many methods, the chosen techniques as following [5]:
- evaporation of metals and condensation of vapour on chilly base,
- chemical sputtering,
- chemical vapour deposition
- mechanical alloying,
- high-energy milling,
- melt spinning.

Based on selected methods of producing amorphous materials, it is important to know that changing of structure from liquid state to solid state without crystallization process could be realized by method of rapid solidification of liquid metal. In rapid solidification methods the melt spinning technique is very useful to manufacturing of metallic glasses [6].

Since amorphous materials were prepared in the Au-Si system alloy in 1960 many scientific investigations have been done. These facts have been informed that amorphous alloys have new atomic configurations, which differ from crystalline alloys [7].

Structural features of amorphous materials have determined many characteristics such as good mechanical properties, useful magnetic properties and unique chemical properties, which have not been achieved from crystalline materials [8].

The general definition presented in [3,5,9] describes metallic glasses (MGs) as metals or alloys of metals, which after critical cooling rates pass from the liquid to the solid state with an amorphous structure.

It is important to known that preparation of conventional glassy alloys requires high critical cooling rates of about 10^4 - 10^6 K/s. Critical cooling rate is necessary to determine a glass-forming ability (GFA) and to produce metallic glasses [8].

According to different cooling rates, the liquid metal during solidification process has amorphous or crystalline structure. Viscosity (η), volume (V) and inner energy (U) of solidified metal during cooling process is changing in discontinuous way (Fig.2). The glass transformation is going in narrow range of temperature defined as glass transition temperature (T_g) [5,10].
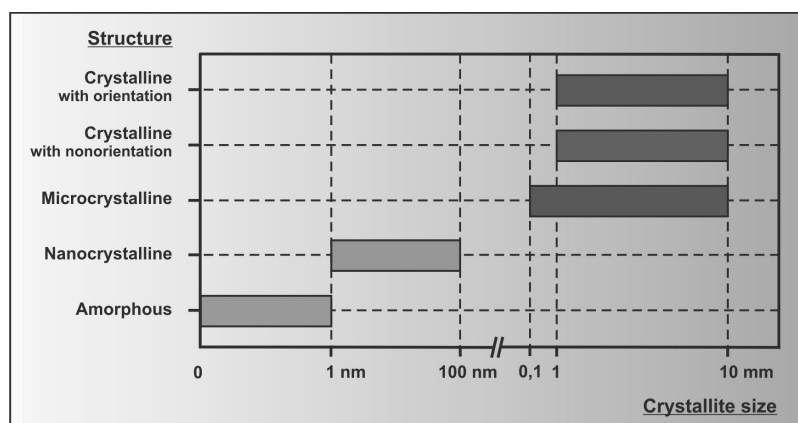
Fig. 1. Classification of materials structure based on crystallite size [2]
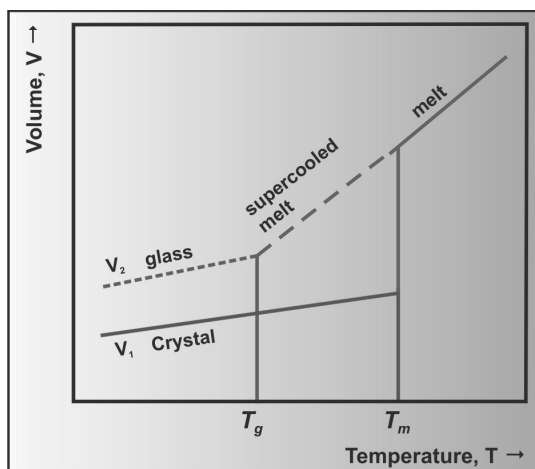
Fig. 2. Schematic diagram of the temperature dependence of volume [5]

Metallic glasses have higher density than crystalline materials. The difference in density is a result of free volumes, which are formed during cooling of molten alloy. The free volumes are responsible for time and temperature instabilities of metallic glasses [5].

Since 1990s, a number of glass-forming systems with excellent GFA in the La- [11], Zr- [12-16], Pd- [17], Ti- [18], Co- [19], Ni- [20] and Fe- [21-23] have been found successfully, which enable the preparation of bulk specimens with dimensions in the millimeter-range by conventional metallurgical casting methods.

The discovery of bulk metallic glasses (BMGs) has caused new interest in research on glassy metals. Before the development of BMG materials there have been many limitations of using metallic glasses, mainly limitation of size and workability. The problem of size and forming has been solved by discovery of bulk metallic glasses, which have a wide supercooled liquid region and high glass-forming ability (Fig.3) [24-27].
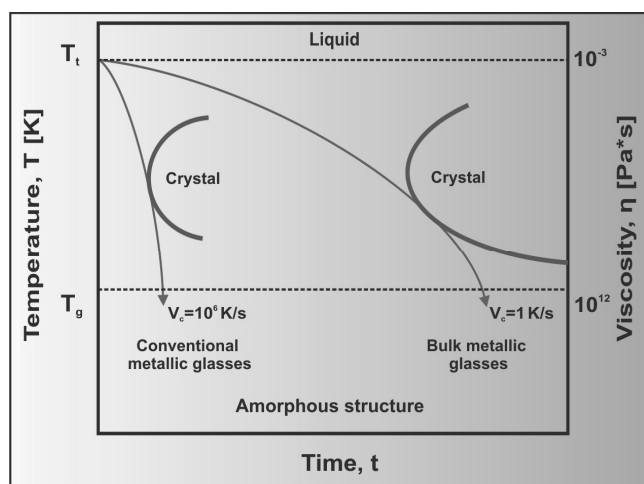
Fig. 3. A comparison of critical cooling rate for conventional and bulk metallic glasses [28]

The bulk amorphous alloy systems can be divided into nonferrous and ferrous types. It is important that bulk amorphous alloys can be fabricated in specified engineering alloy systems such as Fe-, Co-, Ni-, Mg-, Ti- and Zr-bases. The maximum diameter of the bulk amorphous alloys tends to increase in the order of Pd-Cu > Zr > Ln = Mg > Fe > Ni > Co = Ti systems [29]. Table 1 presents the bulk amorphous alloy systems reported up to date with the years, when each alloy system was reported.

Fe-based bulk metallic glasses with critical cooling rates below 10^3 K/s have been often found in Fe-based alloy systems containing metalloids (B, C, Si, and P) and early transition elements (Zr, Nb, Hf). The first Fe-based bulk glassy alloys were prepared in 1995, since then, a variety of Fe-based bulk glassy alloys have been prepared [30].

The Fe-based metallic glasses are studied as an interesting class of engineering materials, which have good soft magnetic properties. Those properties are attractive compared with conventional crystalline alloys and they are very useful in a wide range of technical applications [5].

Table 1.
Alloy systems, years and maximum casting thickness of new multicomponent alloys with high glass-forming ability [7]

g_{max}/mm	Nonferrous alloy systems	Years
10	Mg-Ln-M	1988
10	Ln-Al-TM	1989
10	Ln-Ga-TM	1989
30	Zr-Al-TM	1990
3	Ti-Zr-TM	1993
25	Zr-Ti-TM-Be	1993
30	Zr-(Ti,Nb,Pd)-Al-TM	1995
72	Pd-Cu-Ni-P	1996
g_{max}/mm	Ferrous alloy systems (Fe-,Co-,Ni-bases)	Years
3	Fe-(Al,Ga)-(P,C,B,Si,Ge)	1995
3	Fe-(Nb,Mo)-(Al,Ga)-(P,B,Si)	1995
1	Co-(Al,Ga)-(P,B,Si)	1996
5	Fe-(Zr,Hf,Nb)-B	1996
1	Co-(Zr,Hf,Nb)-B	1996
1	Ni-(Zr,Hf,Nb)-B	1996
1	Fe-Co-Ln-B	1998
2	Fe-(Nb,Cr,Mo)-(C,B)	1999
	Ln – lanthanide metal, TM – transition metal	

Unique properties of bulk metallic glasses caused that this materials are adopted for applications in many fields and they will be more significant engineering materials in the future (Tab.2).

Bulk metallic glasses are a novel class of engineering materials, which have unique mechanical, thermal, magnetic and corrosion properties. That properties are attractive compared with conventional crystalline alloys and are very useful in wide range of engineering applications [31].

Table 2.
Main properties and applications of bulk metallic glasses [31]

Properties	Applications
High strength	Machinery materials
High hardness	Optical precision materials
High fracture toughness	Die materials
High impact fracture energy	Tool materials
High fatigue strength	Cutting materials
High corrosion resistance	Corrosion resistant materials
High wear resistance	Hydrogen storage materials
High reflection ratio	Composite materials
Good soft magnetism	Writing appliance materials
High magnetostriction	Bonding materials

Inoue at el. based on the multicomponents of glassy alloys with high GFA have proposed empirical rules (Fig.4) for [8]:
- achieving high glass-forming ability,
- low critical cooling rate,
- maximum amorphous sample thickness.

These rules have informed that multicomponent alloy should consist of [25-27]:
- more than three elements,
- the alloy should contain two or more metallic elements with different atomic sizes,
- the metallic elements should have large negative heats of mixing with the metalloid type of components,
- the alloy should be eutectic.
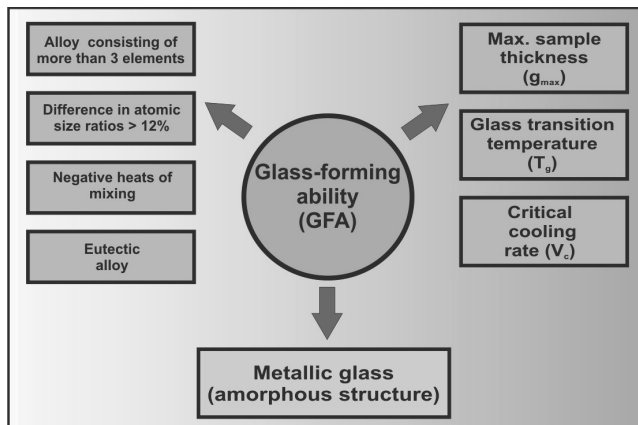
Fig. 4. Schematic correlation between high glass-forming ability, glass transition temperature, maximum sample thickness and critical cooling rate of metallic glasses [32]

The glass-forming ability of bulk metallic alloys depends on temperature difference (ΔT_x) between glass transition temperature (T_g) and crystallisation temperature (T_x). The increase of ΔT_x causes the decrease of critical cooling rate (V_c) and growth of maximum thickness of bulk metallic glasses (Fig.5) [28].
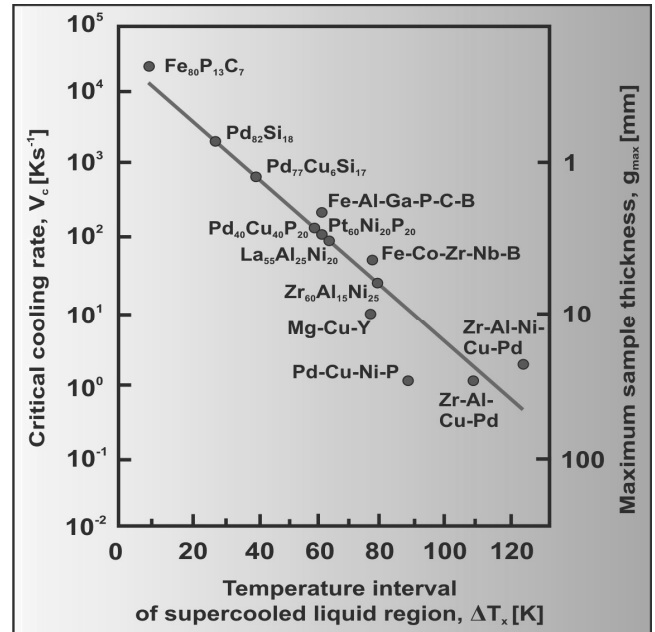
Fig. 5. Relationship between the critical cooling rate for glass formation (V_c), the maximum sample thickness (g_{max}) and the temperature interval of supercooled liquid region (ΔT_x) [24]

Table 3.
Parameters of glass-forming ability of some bulk amorphous alloys based on Fe, Cu, Ti, Zr, Mg [33]

Alloy	T_{rg}	K_{gl}	S	ΔT_x [K]
$Fe_{72}Al_5Ga_2P_{11}C_6B_4$	0.58	0.13	1.00	61
$Cu_{47}Ti_{34}Zr_{11}Ni_8$	0.58	0.10	0.55	46
$Ti_{50}Cu_{25}Ni_{20}Co_5$	0.54	0.20	1.97	90
$Ti_{50}Cu_{30}Ni_{15}Co_5$	0.54	0.09	0.69	47
$Ti_{50}Cu_{40}Ni_5Co_5$	0.54	0.11	0.69	55
$Zr_{55}Al_{20}Ni_{25}$	0.62	0.19	1.90	74
$Zr_{66}Al_8Ni_{26}$	0.56	0.11	0.94	52
$Zr_{66}Al_9Cu_{16}Ni_9$	0.59	0.19	2.23	72
$Zr_{66}Al_8Cu_7Ni_{19}$	0.58	0.27	2.13	99
$Zr_{60}Al_{10}Ni_{10}Cu_{15}Pd_5$	0.58	0.20	2.39	82
$Mg_{50}Ni_{30}Y_{20}$	0.60	0.14	0.65	41
$Mg_{65}Cu_{25}Y_{10}$	0.60	0.27	1.00	61
$Mg_{79.4}Ni_{10.4}Nd_{10.2}$	0.65	0.05	0.28	12
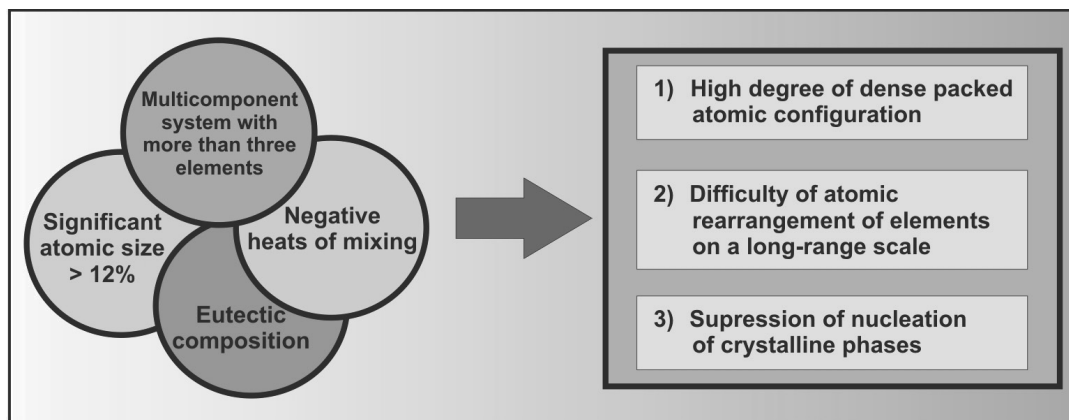
Fig. 6. Features of alloys components for reduced instability of supercooled liquid region and high glass-forming ability [7]
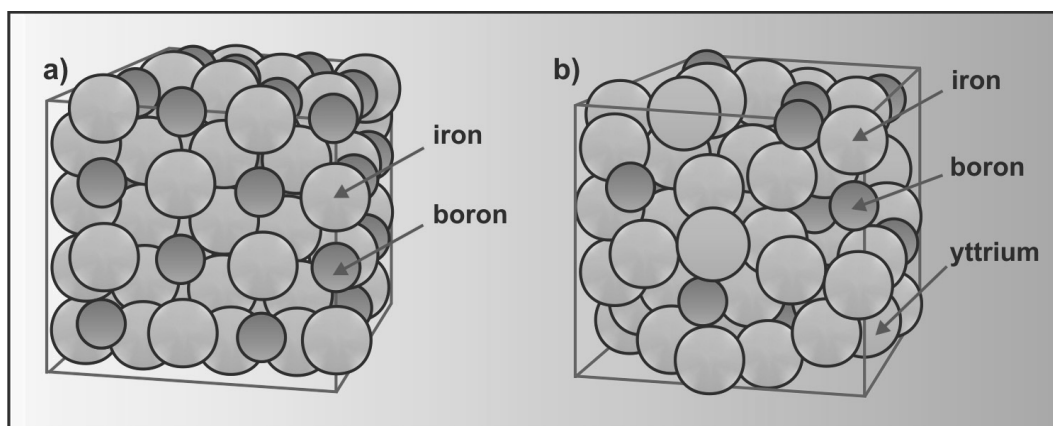
Fig. 7. Schematic models of atoms arrangements in: a) binary alloy Fe-B, b) ternary alloy Fe-Y-B [37]

Table 3 presents several parameters often used to determine the glass-forming ability of some bulk amorphous alloys based on Fe, Cu, Ti, Zr, Mg.

The first of all is parameter defined as the reduced glass transition temperature (T_{rg}). The reduced glass temperature is ratio between the glass transition temperature (T_g) and melting point temperature (T_l) [33,34].

The temperature interval (ΔT_x) between the glass transition temperature (T_g) and the onset crystallization temperature (T_x) is another glass-forming ability indificator. This parameter is also called as the supercooled liquid region. It is obviously known that the larger the temperature interval, the higher glass-forming ability [8,35,36].

Figure 6 summarizes the reasons for achieving a high glass-forming ability of multicomponents alloys. It is confirmed that glass-forming ability is necessary to formation of a new kind of supercooled liquid with high degree of dense packed atomic configuration with short-range and long-range atomic interactions resulting from elements with different atomic sizes and negative heat of mixing [7].

The new structure of supercooled liquid can have a higher liquid/solid interfacial energy wanted to the suppression of nucleation of crystalline phases and crystal growth.

Inoue's empirical rules were tested in work [37] by comparative analysis of glass-forming ability for two-element (binary) and three-element (ternary) alloy.

A typical two-element alloy consists of iron atoms (atomic radius = 0.124 nm) and boron atoms (atomic radius = 0.088 nm), which naturally arrange themselves into a crystalline pattern upon cooling. The repeating spaces between the atoms are grain boundaries. Crystals can shift across these boundaries, allowing oxidation and deformation [37].

Introducing a third element with a significantly different atomic radius, in this case large yttrium atoms (atomic radius = 0.181 nm), slow down the alloy's tendency to crystallize, so it solidifies in a random pattern similar to that of glass [37].

The atomic models of different alloys can be simulated in computers, the researchers endless trial and error in their quest for promising amorphous metals.

Crystallization process can be precisely investigated by many experimental methods like differential scanning calorimetry (DSC), X-ray diffraction (XRD) and transmission electron microscopy (TEM). These studies can also provide information for understanding the influence of microstructure changes under heat activation like structural relaxation, nanocrystallization and crystallization on physical properties [38].

The investigation of the crystallization process is important for understanding the mechanisms of phase transformation from equilibrium, the thermal stability of metallic glasses and for producing controlled microstructures. Since the formation of metallic glasses was getting easier, much work has been devoted to their crystallization. However, a proper understanding for the thermal stability against crystallization of the metallic glasses is still lacking [39].

Crystallization under various conditions could be precisely investigated by many methods like differential scanning calorimetry (DSC), differential thermal analysis (DTA), X-ray diffraction (XRD), neutron scattering, density and acoustic measurements. That studies could also provide information for understanding the influence of microstructure changes on physical properties during relaxation, nanocrystallization and crystallization processes [38].

In general, the scheme of crystallization process of metallic glasses is following. At the initial stage of crystallization process, there are formed metallic elements and their solutions. When the process is more advanced, there are formed borides of metal and intermetallic phases [5].

Table 4 presents examples of crystallization's products of chosen Fe-based metallic glasses.

Table 4.
Products of crystallization of Fe-based metallic glasses [5]

Glassy alloy	Products of crystallization process
$Fe_{75}Si_{15}B_{10}$	α-Fe(Si), Fe_3B, Fe_2B, Fe_3Si
$Fe_{77.5}Si_{13.5}B_9$	α-Fe(Si), Fe_3B
$Fe_{70}Cr_{18}B_{10}Ti_2$	α-Fe, $(Fe,Cr)_3B$
$Fe_{81}Si_{13.5}B_{13.5}C_2$	α-Fe(Si,C), Fe_3B, Fe_2B
$Fe_{76.5}Cu_1Si_{13.5}B_9$	α-Fe(Si)
$Fe_{73.5}Cu_1Ta_3Si_{13.5}B_9$	α-Fe(Si), Fe_3Si
$Fe_{73.5}Cu_1Nb_3Si_{13.5}B_9$	α-Fe(Si), Fe_3Si
$Fe_{73.5}Si_{13.5}B_9Nb_3Cu_1$	α-Fe, Fe_3B, $Fe_{23}B_6$, Fe_2B
$Fe_{74.5}Nb_3Si_{13.5}B_9$	α-Fe(Si), Fe_3B
$Fe_{75}Co_3Si_9B_{13}$	α-Fe, $(Fe,Co)_3B$, $(Fe,Co)_2B$,
$Fe_{76}Cr_2Si_8B_{14}$	α-Fe(Si), Fe_3Si, Fe_3B, Fe_2B
$Fe_{76}Mo_2Si_8B_{14}$	α-Fe(Si), Fe_3Si, Fe_3B, FeMo
$Fe_{86}Zr_7Cu_1B_6$	α-Fe

Improving of magnetic properties (magnetic permeability) of metallic glasses is a result of formation a nanocrystalline phase. What is important, the enhancement of magnetic permeability is also could be explained by decrease of magnetostriction constant and annealing out of microvoids (Fig.8) [40,41].
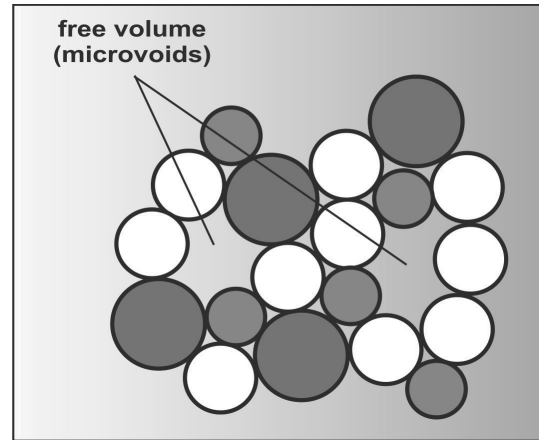
Fig. 8. Schematic illustration of structure defects identified as agglomerates of the free volume which are formed during the rapid quenching process [40]

Figure 9 shows the plot of the intensity of magnetic after-effect determined at room temperature against annealing temperature for Fe-based metallic glasses. $\Delta\mu/\mu$ is directly proportional to the concentration of migrating defects, i.e. microvoid concentration [42-48]. It is clear that magnetic after-effect curves exhibit a maximum near 350 - 450K (coagulation process of microvoids) and at higher temperatures a drastic decrease of $\Delta\mu/\mu$ value indicating annealing out of microvoids.
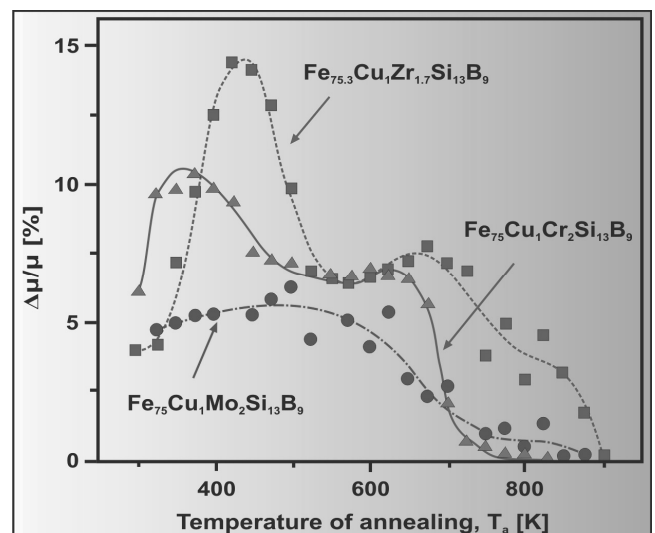
Fig. 9. Magnetic after-effects determined at room temperature versus annealing temperature for selected Fe-based amorphous alloys [42]
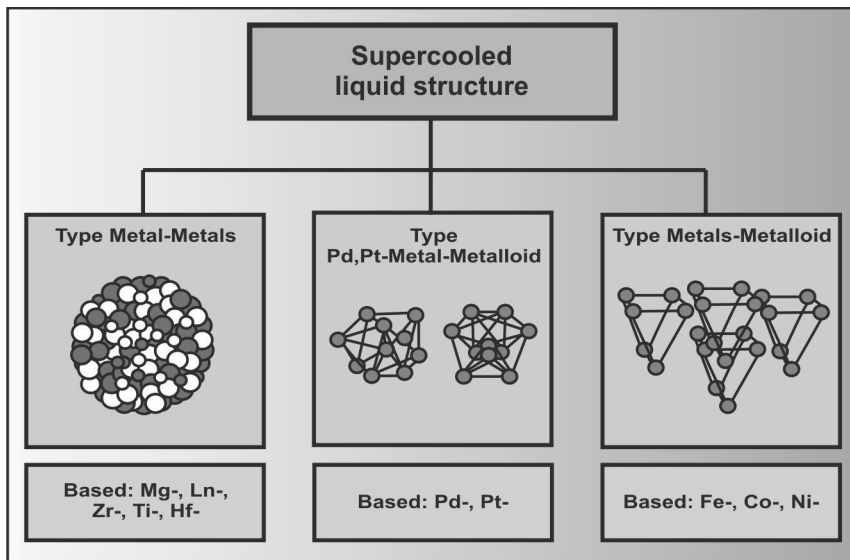
Fig. 10. The different atomic configurations of three types of bulk metallic glasses based on Mg, Ln, Zr, Ti, Hf, Pd, Pt, Fe, Co, Ni [49]

Inoue classified the bulk metallic glasses into three types [49]:
- metal-metals type alloys,
- metals-metalloid type alloys,
- Pd-metal-metalloid type alloys.

In the metal-metals type alloy, TEM, XRD, and neutron diffraction studies reveal that the glass consists of icosahedral clusters (quazicrystals). The critical size for a transition from icosahedral cluster to icosahedral phase is around 8 nm [28].

The quasicystalline phases have non-periodic structure, but they characterized by the long-range arrangements of atoms. These kinds of materials can be situated between amorphous and crystalline materials. Many quasicrystalline phases have been discovered in Al-, Mg- and Ti- based alloys. Figure 11 presents the local structure of Al-Mn quasicrystal [50].

In the metals-metalloid type glassy alloys, for example of Fe(Co)-Nb-B alloy, a network atomic configurations consisting of trigonal prisms which are connected with each other through glue atoms comprising Zr, Nb, Ta or lanthanide metal are commonly found. The local structure atomic model of Fe-TM-B bulk metallic glass is presented in Figure 12. That model is an attempt of describing of Fe-based glassy alloys structure by presentation of probably configurations of atoms [49].

The structural investigation shows that Pd-based bulk metallic glasses consist of two large clustered units of a trigonal prism caped with three half-octahedra for the Pd-Ni-P and a tetragonal dodecahedron for the Pd-Cu-P region [49].

Fig. 11. Local structure atomic model of Al-Mn quasicrystal [50]
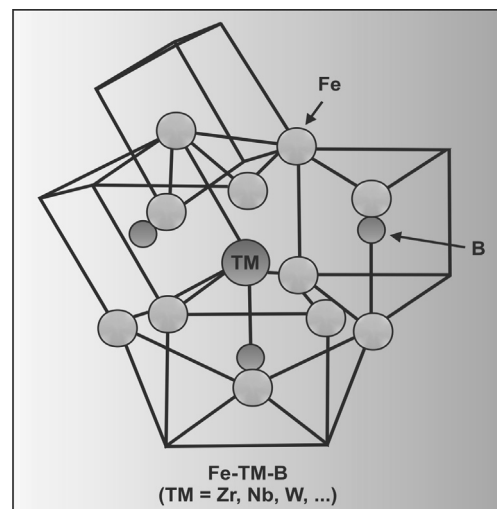
Fig. 12. Local structure atomic model of Fe-based bulk metallic glasses [49]

Structural models for amorphous materials can be classified into two main group [51]:

- models which are based on the theory of the liquid state,
- models which are based on three-dimensional clusters.

The models based on the theory of the liquid state are calculated from suitable pair potential functions using one of the existing theoretical equations. The most well known model of that group is a hard-sphere model for which the potential is given by repulsion between the atoms.

However, the most of the models for metallic glasses belong to the class includes three-dimensional clusters. The clusters are defined as a set of coordinates of several thousand atoms which are constructed using computer methods. The clusters contain more structural information than experimental functions (for example about local symmetries, bond angles).

What is important, the cluster models may serve as a basis for the calculation of the other physical properties such as electric and mechanical properties of a glassy material, which again can be compared with experimental data.

The development of a proper cluster model includes two main steps [51]:

- construction of an initial set of atomic positions as a starting structure,
- refinement of the structure.

The classification of existing cluster models is not easy but the rough classification can includes [51]:

- dense random packing of hard sphere (DRPHS),
- stereochemically defined models (SCD),
- molecular dynamics calculations (MD),
- Monte Carlo simulations (MC).

The DRPHS and SCD models require a construction of the starting cluster as the first step of model building, but for the MC and MD models a refinement is the essential procedure.

The DRPHS models show the main features such as atomic distance and the characteristic peak splitting in the atoms pairs correlation, but a comparison between experiment and model is poor. In SCD models no single atoms can be packed together but structural units consisting of several atoms which already have stereochemically defined short-range order. However, in MD models not only positions but also velocities of atoms are necessary to built a starting model. The development of the model contains a solving of the Newtonian equations of motion using selected pair potentials. To simulate procedure from a liquid to an amorphous state the velocities of the atoms are reduced.

The first Fe-based bulk glassy alloys were prepared in 1995, since then, a variety of Fe-based bulk glassy alloys have been formed and their alloy components can be classified into five groups (Table 5). It is important to know that Fe-based bulk metallic glasses with high strength of over 3300 MPa can be obtained only in two alloy groups of I and IV [30].

Figure 13 and 14 present some X-ray diffraction patterns of Fe-based bulk amorphous alloys as glassy rods with diameter from 2.5 to 5 mm for Fe-Co-B-Si-Nb alloy and from 3 to 4 mm for similar alloy composition with Ni addition.

Table 5.
Classification of Fe-based bulk metallic glasses [30]

Group	Examples of Fe-based glassy alloys
I.	Fe-(Al,Ga)-(P,C,B,Si) Fe-(Cr,Mo,Nb)-(P,C,B,Si) Fe-Ga-(P,C,B,Si)
II.	Fe-(Zr,Hf,Nb,Ta)-B
III.	Fe-(Cr,Mo)-(C,B)
IV.	Fe-B-Si-Nb Fe-Co-B-Si-Nb Fe-Co-Ni-B-Si-Nb
V.	Fe-Nd-Al
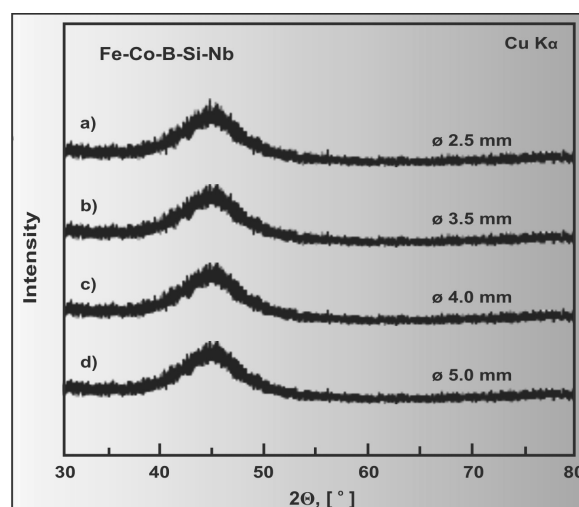
Fig. 13. X-ray diffraction patterns of Fe-Co-B-Si-Nb glassy rods in as-cast state with diameter from 2.5 to 5 mm [52]
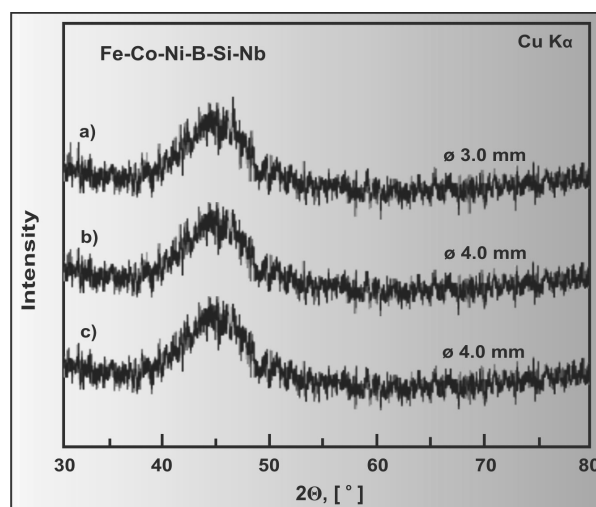
Fig. 14. X-ray diffraction patterns of Fe-Co-Ni-B-Si-Nb glassy rods in as-cast state with diameter from 3 to 4 mm [53]
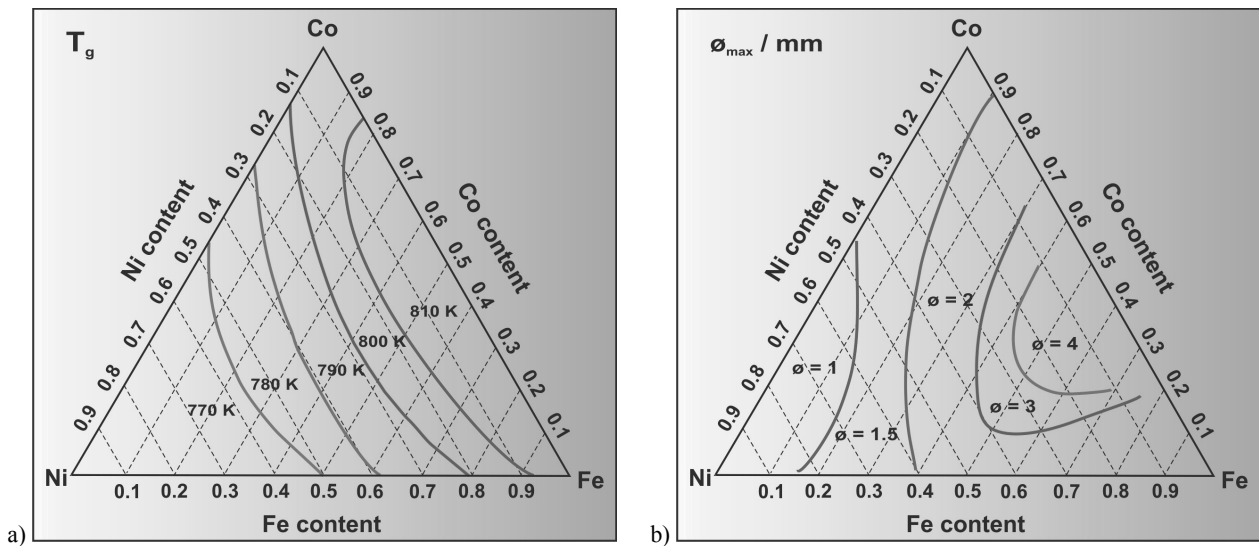
Fig. 15. Compositional dependence of the reduced glass transition temperature (a) and maximum diameter for amorphous structure formation (b) for Fe-Co-Ni-B-Si-Nb glassy alloys [54,55]

Figure 15a shows the compositional dependence of the glass transition temperature (T_g) of the (Fe,Co,Ni)-B-Si-Nb metallic glasses. The T_g indicates an important change with Ni content and decreases almost linearly from 810 to 770 K with increasing Ni content. There is no distinct difference in glass transition temperature with the concentration ratio of Co to Fe [54].

A compositional dependence of the diameter of studied metallic glasses in form of rods is presented in Figure 15b. The amorphous structure was obtained only in the diameter of 1 mm for the alloys in the Ni-rich composition. With the increasing of Fe and Co contents, the diameter of glassy rods increased. Bulk metallic glasses in rod shaped with diameters of 3 and 4 mm were successfully synthesized in the Fe- and Co-rich composition range [55].

In addition, Figure 16 shows the relationship between the maximum rod diameter (g_{max}) for the formation of an amorphous structure, the reduced glass transition temperature (T_{rg}) and the supercooled liquid region (ΔT_x) for Fe-Co-B-Si-Nb and Fe-Co-Ga-P-C-B-Si bulk metallic glasses.

The maximum diameter of studied glassy alloys tends to increase with increasing of T_{rg} and ΔT_x. The distinct tendency indicates that the high glass-forming ability of tested Fe-based alloys is due to the combination of two factors. The first one is the increasing in the viscosity of supercooled liquid with decreasing temperature and last one is the high stability of supercooled solid state with strong suppression of crystallization process resulting from the large atomic size mismatch [30].
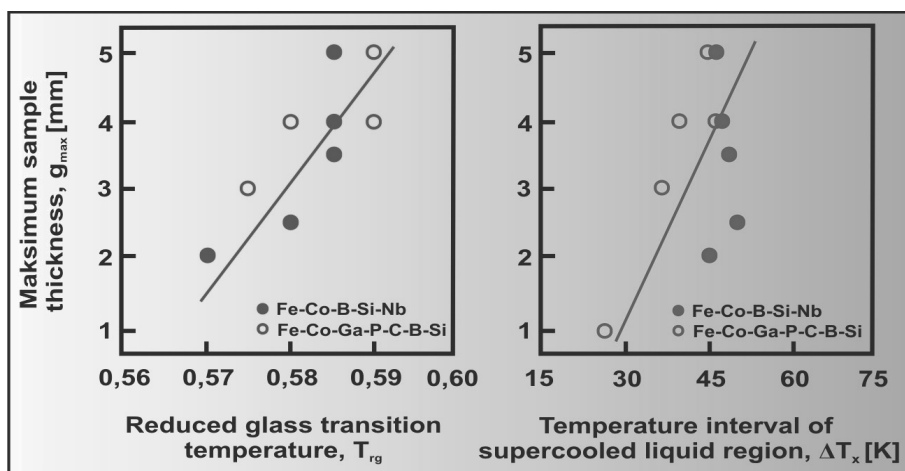
Fig. 16. Relationship between maximum sample thickness with amorphous structure (g_{max}), reduced glass transition temperature (T_{rg}) and the temperature interval of supercooled liquid region (ΔT_x) [30]

2. Material and research methodology

The aim of this paper is the microstructure characterization, thermal stability and soft magnetic properties analysis of $Fe_{72}B_{20}Si_4Nb_4$ bulk amorphous alloy in as-cast state and after heat treatment processing. Investigations were done with use of XRD, TEM, SEM, DSC, DTA and magnetic measurements methods.

The investigated material was cast in form of the ribbons with thickness (g) from 0.03 mm to 0.2 mm and rods with diameter ($\varnothing$) of 1.5 and 2 mm. The ingot was prepared by induction melting of a mixture of pure elements of Fe, Nb, Si and B under protective gas atmosphere.

The ribbon shaped metallic glasses were manufactured by the "chill-block melt spinning" (CBMS) technique, which is a method of continuous casting of the liquid alloy on the surface of a turning copper based wheel [56-61]. The casting conditions include linear speed of copper wheel: 20 m/s and ejection over-pressure of molten alloy: 200 mBar.

The samples cast as rod shaped metallic glasses were manufactured by the pressure die casting method. The pressure die casting technique [62-66] is the method of casting a molten alloy ingot into copper mould under gas pressure (Fig.17).

In order to study structural relaxation and crystallization processes samples in the as-cast state were annealed at the temperature range from 373 to 923 K with the step of 50 K. Tested ribbons were annealed in electric chamber furnace THERMOLYNE 6020C under protective argon atmosphere. The annealing time was constant and equaled of 1 hour.

Structure analysis of studied materials in as-cast state was carried out using Seifert-FPM XRD 7 diffractometer with $Co_{K\alpha}$ radiation for ribbon samples measurements and PANalytical X'Pert diffractometer with $Co_{K\alpha}$ radiation for rod samples examination.

Phase analysis of ribbons after crystallization process were carried out using the X-Pert Philips diffractometer equipped with curved graphite monochromator on diffracted beam and a tube provided with copper anode. It was supplied by current intensity of 30 mA and voltage of 40 kV. The length of radiation ($\lambda Cu_{K\alpha}$) was 1.54178 Å. The data of diffraction lines were recorded by "step-scanning" method in 2θ range from 30° to 90°.

Transmission electron microscopy (TESLA BS 540) was used for the structural characterization of studied samples in as-cast state and after annealing process. Thin foils for TEM observation (from central part of tested samples) were prepared by an electrolytic polishing method after previous mechanical grinding.

The thermal properties associated with crystallization temperature of the amorphous ribbons were measured using the differential thermal analysis (Mettler - DTA) at a constant heating rate of 6 K/s under an argon protective atmosphere.

The differential scanning calorimetry (DSC, SDT Q600) was used to determine crystallization, glass transition temperature and Curie temperature for glassy samples in form of rod. The heating rate of calorimetry measurements was 20 K/min

The Curie temperature of investigated glassy ribbons was determined by measuring a volume of magnetization in function of temperature. The Curie temperature of amorphous phase was calculated from the condition $dM(T)/dT=minimum$ [45].

Magnetic measurements of annealed samples (determined at room temperature) included following properties:

(1) relative magnetic permeability - determined by Maxwell-Wien bridge at a frequency of 1030 Hz and magnetic field H= 0.5 A/m), (magnetic permeability measurements were carried out for ribbons of length of 100 mm);

(2) coercive field - measured by coercivemeter;

(3) magnetic permeability relaxation $\Delta\mu/\mu$ (magnetic after-effects) - determined by measuring changes of magnetic permeability as a function of time after demagnetization, where $\Delta\mu$ is difference between magnetic permeability determined at $t_1 = 30$ s and $t_2 = 1800$ s after demagnetization and μ at t_1 [46-48].

The magnetic hysteresis loops of studied metallic glasses in form of ribbons were measured by the resonance vibrating sample magnetometer (R-VSM) presented by Wrona et al. [67,68]. R-VSM measurements give information about averaged magnetization process from the whole volume of the tested sample, which oscillates in parallel to the direction of external magnetic field.

Experimental procedure of metallic glasses production with stages of master alloy preparing and casting of amorphous materials by different methods is presented in Figure 18.

Master alloy Fe-B-Si-Nb

The pressure die casting equipment

Bulk metallic glasses in form of rods
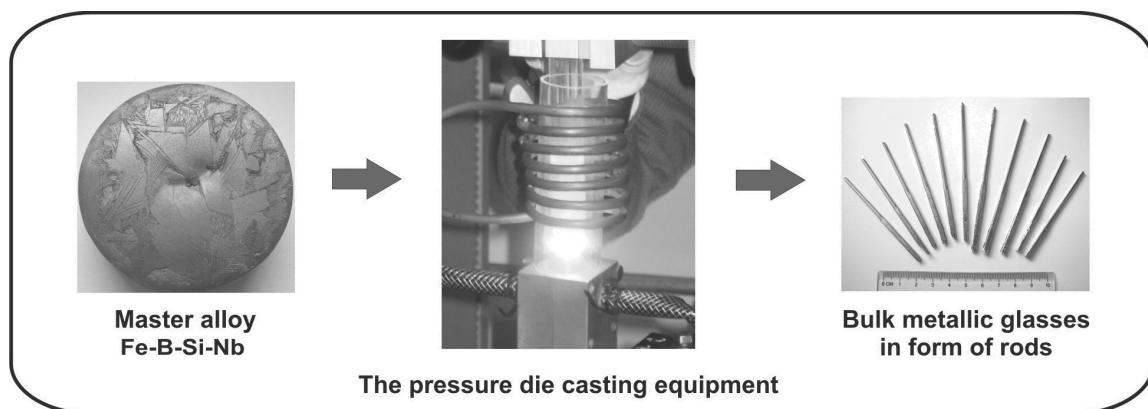
Fig. 17. Schematic illustration of the pressure die casting method used for bulk amorphous samples casting
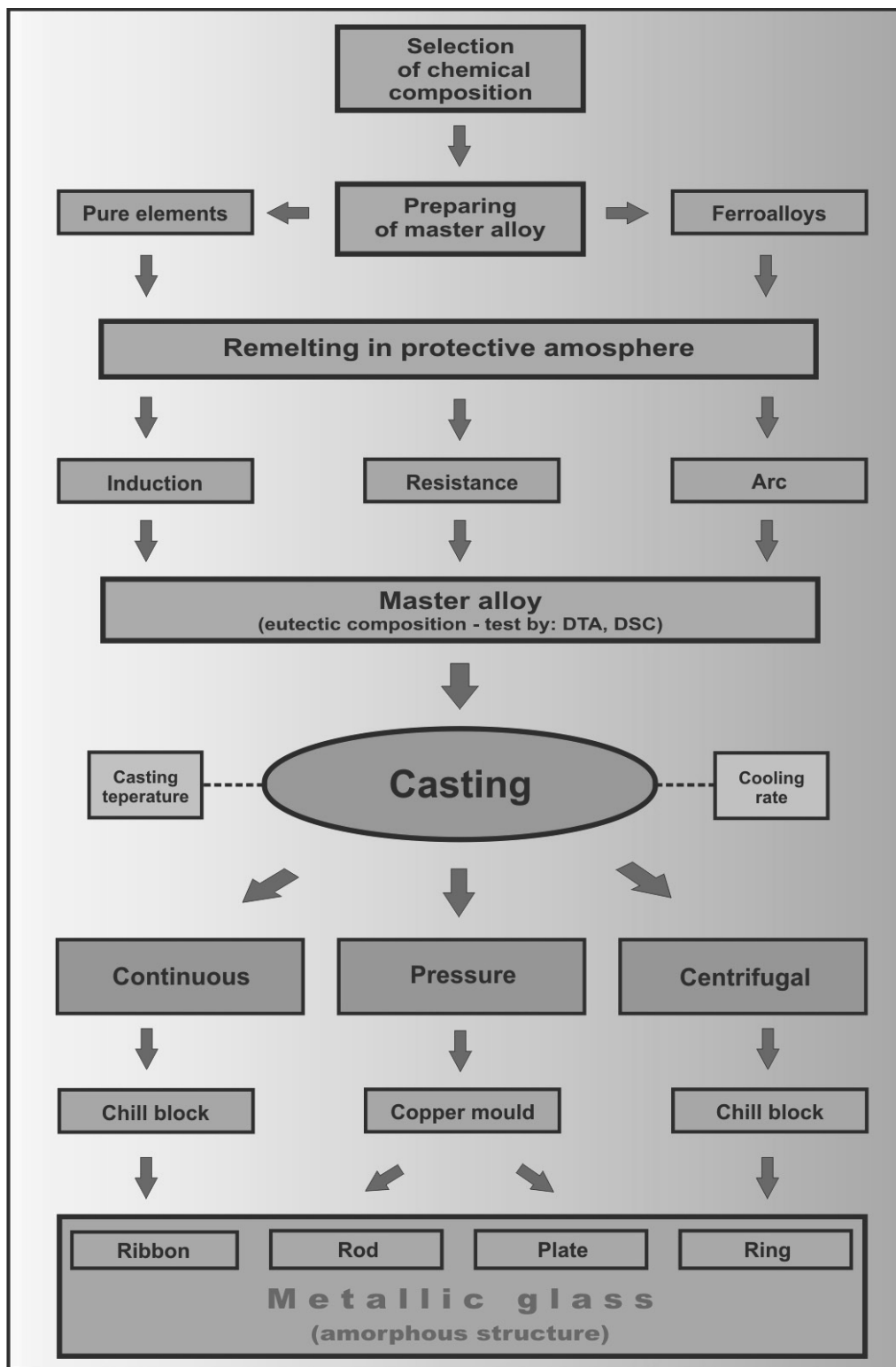
Fig. 18. Experimental procedure of metallic glasses production with stages of master alloy preparing and casting of amorphous materials by different technological methods

3. Results and discussion

The X-ray diffraction investigations reveal that the studied as-cast $Fe_{72}B_{20}Si_4Nb_4$ samples were amorphous. The diffraction patterns of tested ribbons with thickness of 0.03, 0.08 and 0.20 mm show the broad diffraction halo characteristic for the amorphous structure (Fig.19).
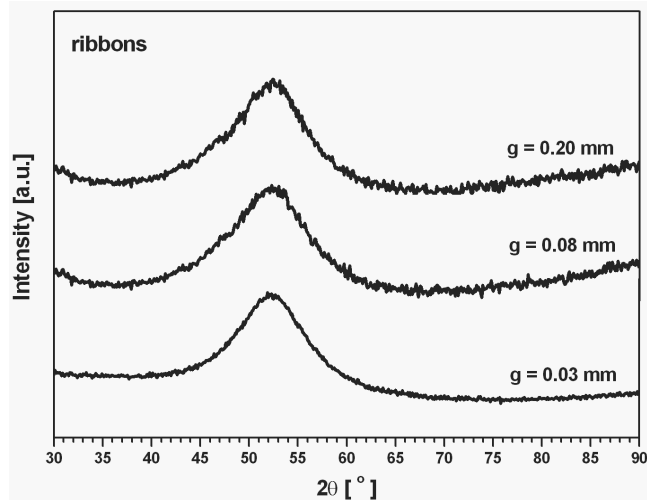
Fig. 19. X-ray diffraction patterns of $Fe_{72}B_{20}Si_4Nb_4$ glassy ribbons in as-cast state with thickness from 0.03 to 0.20 mm

The amorphous structure of studied alloy cast in form of rods with diameter of 1.5 and 2 mm confirmed the diffraction patterns presented in Figure 20.

Figures 21 and 22 show TEM images and electron diffraction patterns of seelcted samples in as-cast state: ribbon with thickness of 0.03 and 0.20 mm and rod with diameter of 1.5 and 2 mm, adequately. The TEM images reveal only a changing of contrast and no appreciable contrast corresponding to a crystalline phase is seen. The electron diffraction pattern consists only of broad diffraction halo rings, which can be seen for all tested samples.
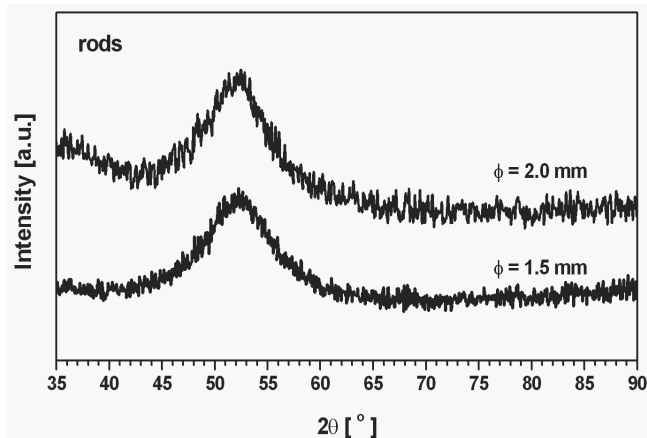
Fig. 20. X-ray diffraction patterns of $Fe_{72}B_{20}Si_4Nb_4$ glassy rods in as-cast state with diameter of 1.5 and 2 mm
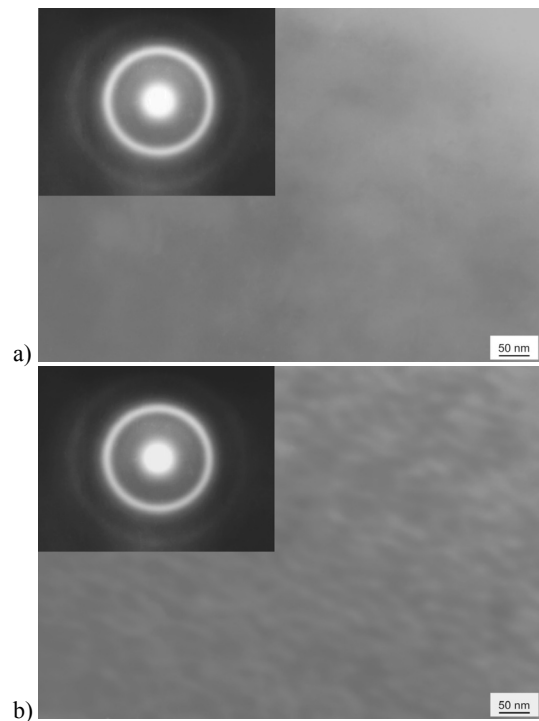
Fig. 21. Transmission electron micrograph and electron diffraction pattern of the as-cast glassy $Fe_{72}B_{20}Si_4Nb_4$ ribbon with a thickness of: (a) 0.03 and (b) 0.20 mm
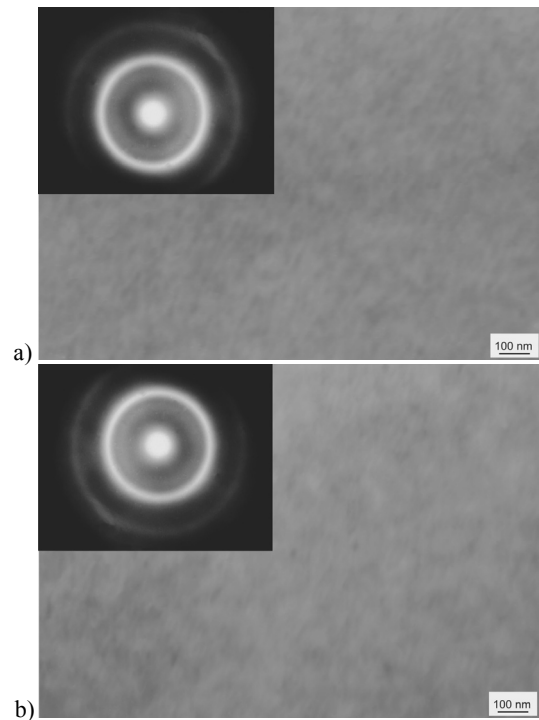
Fig. 22. Transmission electron micrograph and electron diffraction pattern of the as-cast glassy $Fe_{72}B_{20}Si_4Nb_4$ rod with a diameter of: (a) 1.5 and (b) 2 mm

The DTA curves (at 6 K/min) measured on amorphous ribbons with thickness of 0.03, 0.08 and 0.20 mm in as-cast state for studied alloy are shown in Figure 23.

The two stage crystallization process was observed for examined ribbons. The first stage crystallization of $Fe_{72}B_{20}Si_4Nb_4$ alloy for sample with thickness of 0.03 mm includes onset crystallization temperature (T_{x1} = 842 K) and peak crystallization temperature (T_{p1} = 864 K). The analysis of the second crystallization stage allows to determine only peak crystallization temperature (T_{p2}) with value of 892 K, as well.

The first stage of crystallization obtained for ribbon with thickness of 0.08 mm includes onset crystallization temperature at value of T_{x1} = 853 K and peak crystallization temperature at T_{p1} = 869 K. The analysis of the second crystallization stage of studied sample allows to determine peak crystallization temperature, which has a value of T_{p2} = 893 K.

The DTA curve obtained for sample with thickness of 0.20 mm informs that first stage of crystallization includes onset crystallization temperature at value of T_{x1} = 857 K and peak crystallization temperature at value of T_{p1} = 871 K. The second crystallization stage of studied ribbon is described by peak with temperature of T_{p2} = 890 K.

The analysis of crystallization process of examined ribbons shows that peak of crystallization temperature peak increases with increasing samples thickness during first stage of crystallization and decreases during second stage of crystallization. The differences of crystallization temperature between ribbons with chosen thickness of the same alloy are probably caused by different amorphous structures as a result of the different cooling rates in casting process of studied metallic glasses.

The DSC curves (at 20 K/min) obtained for amorphous rods with diameter of 1.5 and 2 mm in as-cast state for $Fe_{72}B_{20}Si_4Nb_4$ alloy are shown in Figure 24. Results of DSC investigations for studied samples confirmed that crystallization temperature increase from 860K to 861K with increasing of sample diameter from 1.5 to 2 mm. It could be an another reason for changing the amorphous structure with sample thickness (critical cooling rate).

The DSC examinations of rod with diameter of 1.5 mm allow to determine the peak crystallization temperature, which has a value of T_{p1} = 884 K and the glass transition temperature (T_g = 817 K). Similarly, for sample with diameter of 2 mm: the peak crystallization temperature is T_{p1} = 885 K and the glass transition temperature reached a value of T_g = 825 K, as well.

Furthermore, the DSC investigations allow to determine Curie temperature (T_c) for studied glassy rods. The Curie temperature (T_c) of rod with diameter of 1.5 mm has a value of 567 K and for sample with diameter of 2 mm, T_c = 570 K (Fig.20). Determined variation of the Curie temperature and crystallization temperature is probably due to different amorphous structures of the tested glassy samples caused by different casting methods (cooling rates).

The crystallization temperatures obtained from DTA and DSC curves are connected with thermal properties of studied bulk metallic glass in form of ribbons and rods in as-cast state.
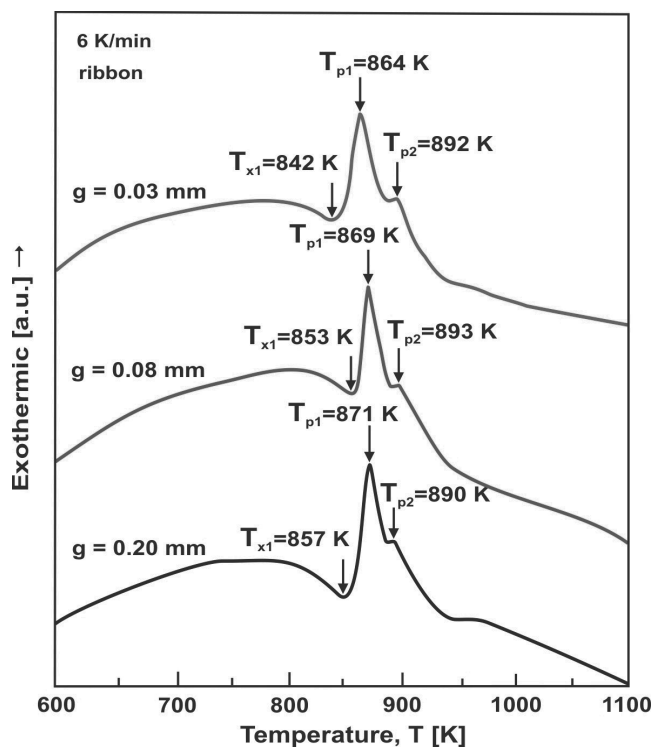
Fig. 23. DTA curves of $Fe_{72}B_{20}Si_4Nb_4$ glassy alloy ribbons in as-cast state (heating rate 6 K/min)
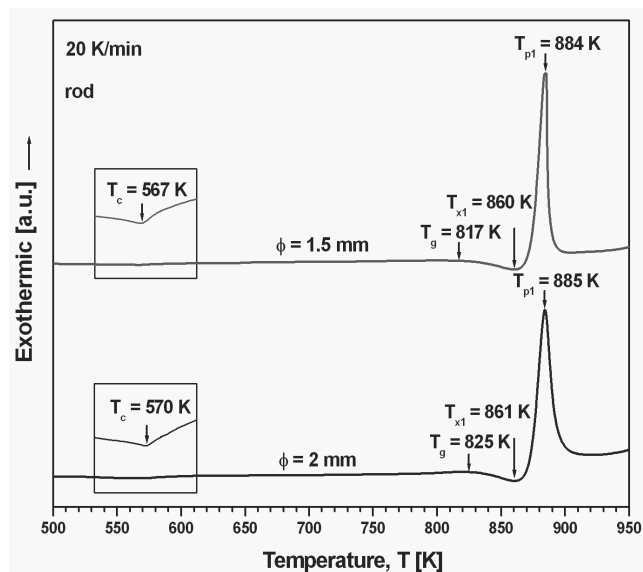
Fig. 24. DSC curves of $Fe_{72}B_{20}Si_4Nb_4$ glassy alloy rods in as-cast state (heating rate 20 K/min)

The selected thermal stability properties like onset and peak crystallization temperature of studied glassy alloy for samples in ribbons and rods form are presented in Table 6.

Table 6.
Thermal properties of $Fe_{72}B_{20}Si_4Nb_4$ bulk metallic glass in ribbons and rods form

Form of sample	Thickness [mm]	Thermal properties		
		T_{x1} [K]	T_{p1} [K]	T_{p2} [K]
Ribbon	0.03	842	864	892
	0.08	853	869	893
	0.20	857	871	890
Rod	1.5	860	884	-
	2.0	861	885	-

Figures 25 - 27 show X-ray diffraction patterns obtained for studied alloy in form of ribbon with thickess of 0.03 mmafter annealing at 823, 873 and 923 K for 1 hour.

The annealing process realized at mention temperatures obviously causes formation of crystalline phases. Qualitative phase analysis from X-ray data enables the identification of a single phase of α-Fe for sample annealed at 823 K. The precipitations for the ribbon annealed at 873 K corresponding to the temperature above the peak crystallization temperature of the first exothermic peak are a mixture of Fe_2B, Fe_3B and $Fe_{23}B_6$ and α-Fe phases. It was also confirmed that the structure after annealing for 1 hour at 923 K corresponding to the temperature above the second exothermic peak consisted of α-Fe phase and borides Fe_2B, Fe_3B and $Fe_{23}B_6$. The X-ray diffraction investigations allow to detection Nb_3Si phases in samples annealed at 873 and 923 K.

Figures 28 - 30 show X-ray diffraction patterns obtained for studied alloy after annealing at 373, 573 and 773 K for 1 hour. It is noticed, that annealing in studied temperature range does not lead to a formation of any crystallites detectable by X-ray diffraction and TEM images. Comparison of diffraction patterns of studied alloy after annealing from 373 K to 773 K shows the narrowing of diffraction lines and increase of their intensity. What is more, the TEM images reveal only a changing of contrast of amorphous phase. These effects indicate that annealing process causes structural relaxation of tested amorphous materials, which leads to changes in their physical properties. These changes are probably due to atomic rearrangements that lead to changes in free volume [4].

Figure 31 - 33 show the transmission electron micrographs plus electron diffraction patterns and their solutions obtained for ribbons of studied alloy after annealing at 823, 873 and 923 K for 1 hour. The annealing process at temperature from 823 K to 923 K obviously causes formation of the crystalline phases. The phase analysis performed from the electron diffraction patterns enables the identification of α-Fe phase and iron borides - Fe_3B.
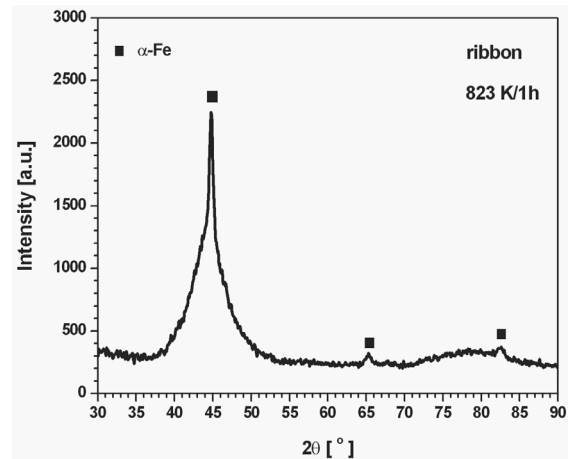
Fig. 25. X-ray diffraction patterns of $Fe_{72}B_{20}Si_4Nb_4$ alloy (ribbon with thickness of 0.03mm) after annealing at 823 K for 1 hour
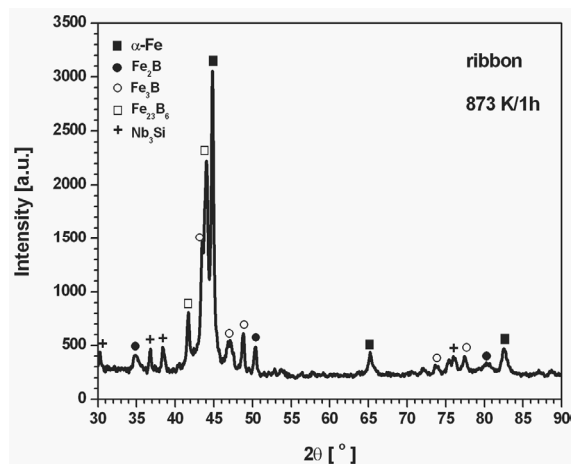
Fig. 26. X-ray diffraction patterns of $Fe_{72}B_{20}Si_4Nb_4$ alloy (ribbon with thickness of 0.03 mm) after annealing at 873 K for 1 hour
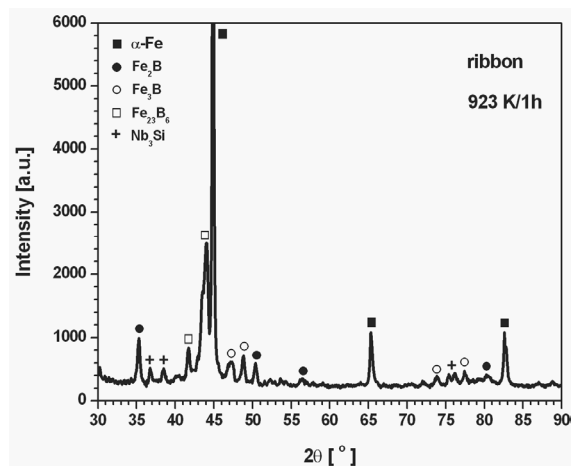
Fig. 27. X-ray diffraction patterns of $Fe_{72}B_{20}Si_4Nb_4$ alloy (ribbon with thickness of 0.03 mm) after annealing at 923 K for 1 hour
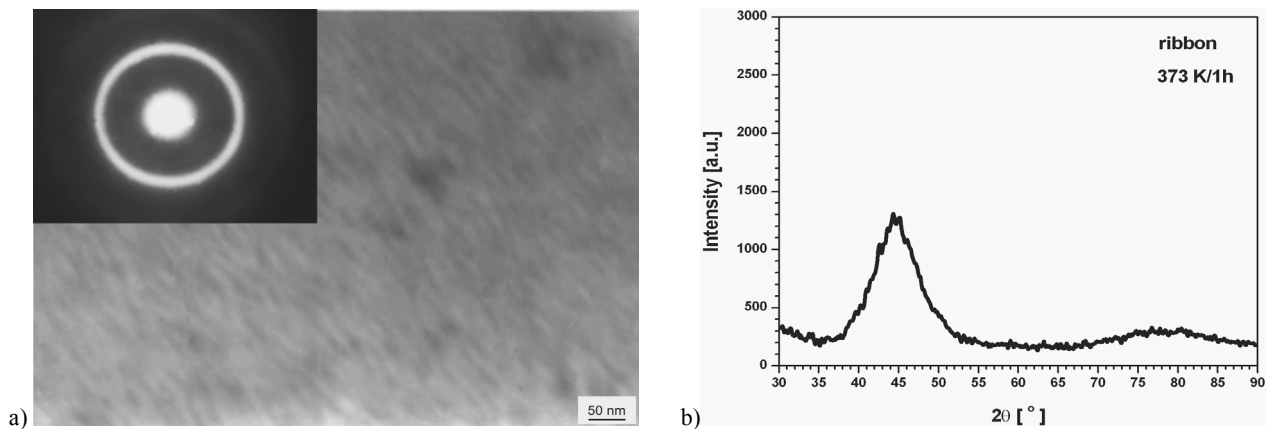
Fig. 28. Transmission electron micrograph and electron diffraction pattern (a) and X-ray diffraction pattern (b) of $Fe_{72}B_{20}Si_4Nb_4$ alloy in form of ribbon with thickness of 0.03mm after annealing at 373 K for 1 hour
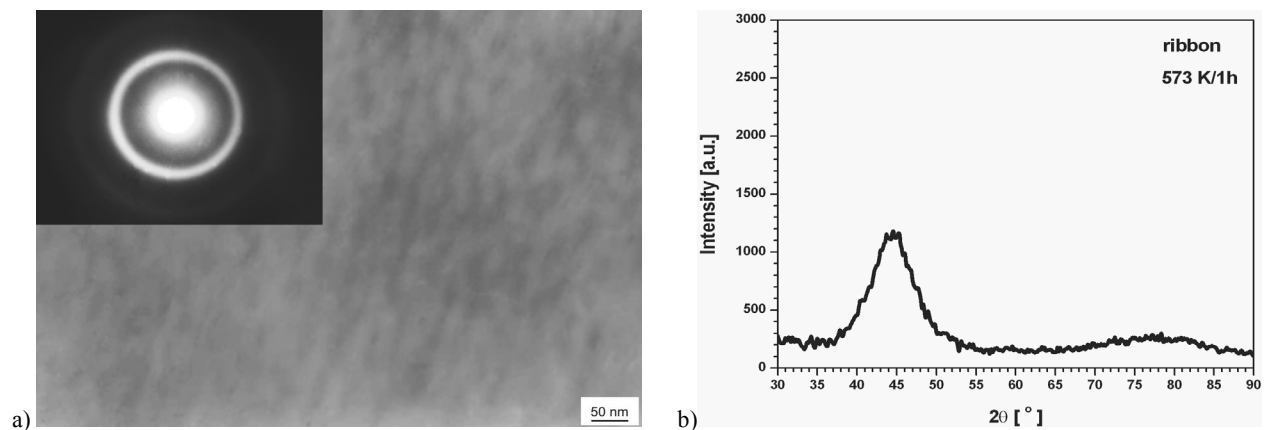
Fig. 29. Transmission electron micrograph and electron diffraction pattern (a) and X-ray diffraction pattern (b) of $Fe_{72}B_{20}Si_4Nb_4$ alloy in form of ribbon with thickness of 0.03 mm after annealing at 573 K for 1 hour
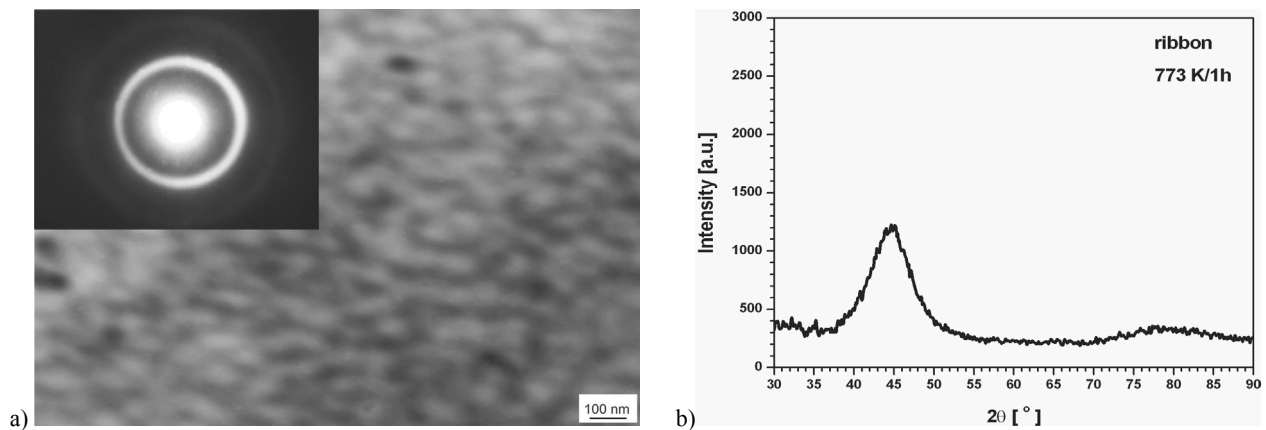
Fig. 30. Transmission electron micrograph and electron diffraction pattern (a) and X-ray diffraction pattern (b) of $Fe_{72}B_{20}Si_4Nb_4$ alloy in form of ribbon with thickness of 0.03 mm after annealing at 773 K for 1 hour
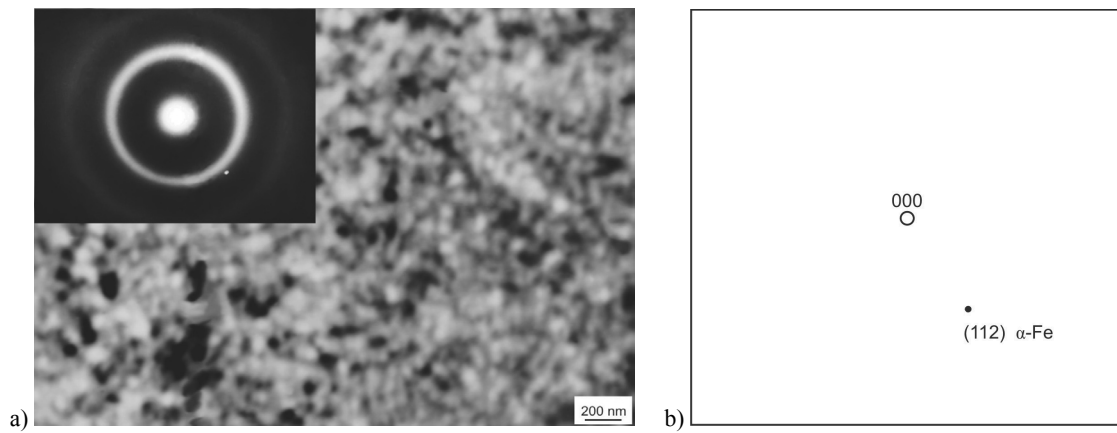
Fig. 31. Transmission electron micrograph plus electron diffraction pattern (a) and solution of diffraction pattern (b) of $Fe_{72}B_{20}Si_4Nb_4$ alloy in form of ribbon with thickness of 0.03 mm after annealing at 873 K for 1 hour
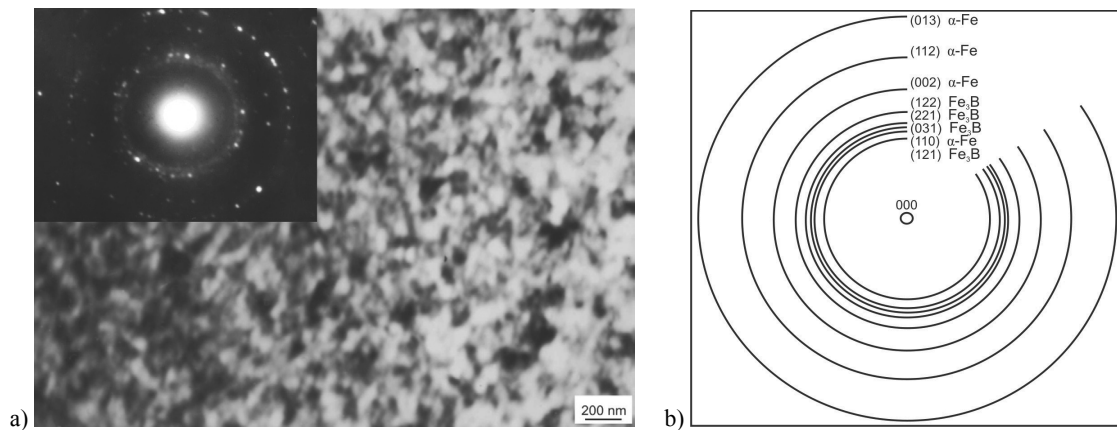
Fig. 32. Transmission electron micrograph plus electron diffraction pattern (a) and solution of diffraction pattern (b) of $Fe_{72}B_{20}Si_4Nb_4$ alloy in form of ribbon with thickness of 0.03 mm after annealing at 873 K for 1 hour
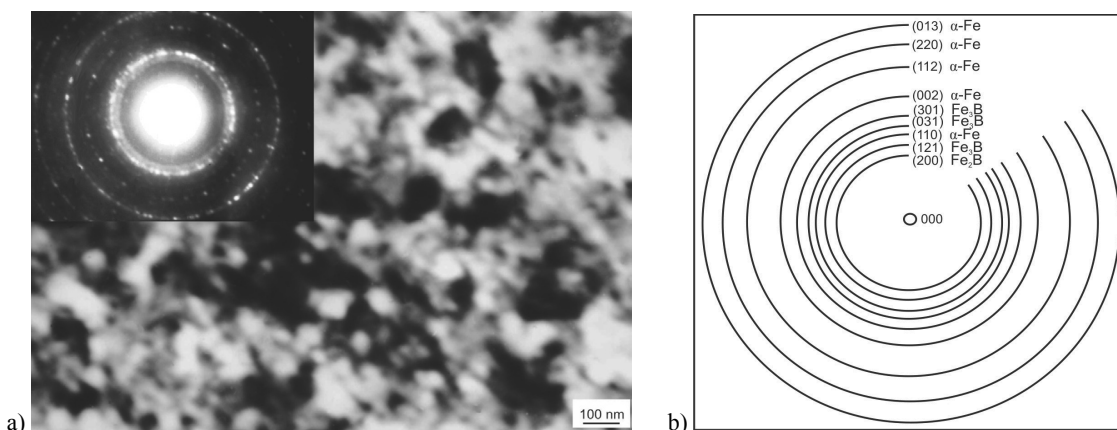
Fig. 33. Transmission electron micrograph plus electron diffraction pattern (a) and solution of diffraction pattern (b) of $Fe_{72}B_{20}Si_4Nb_4$ alloy in form of ribbon with thickness of 0.03 mm after annealing at 923 K for 1 hour
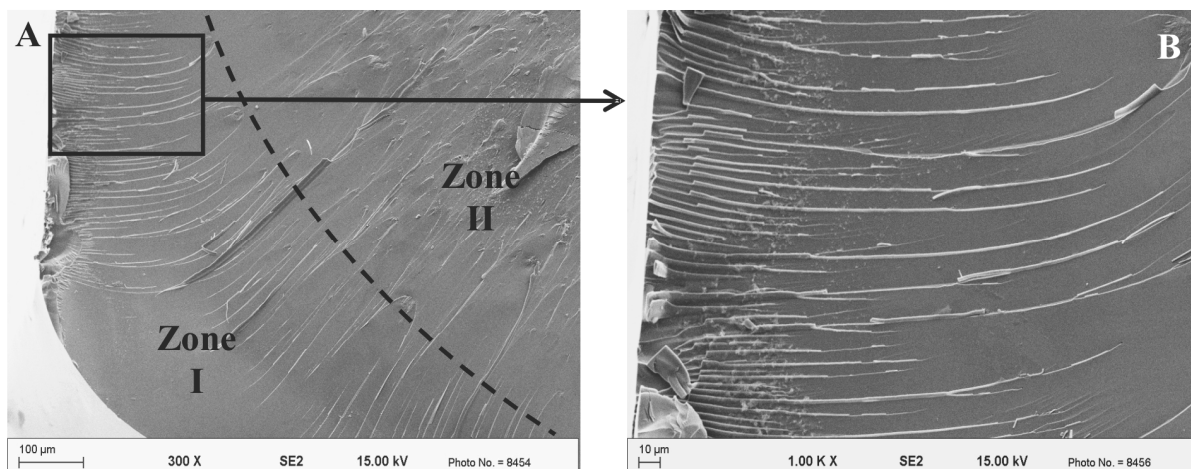
Fig. 34. SEM micrographs of the fracture morphology of $Fe_{72}B_{20}Si_4Nb_4$ amorphous rod in as-cast state with diameter of 1.5 mm: A – magn. 300x, B – magn. 1000x
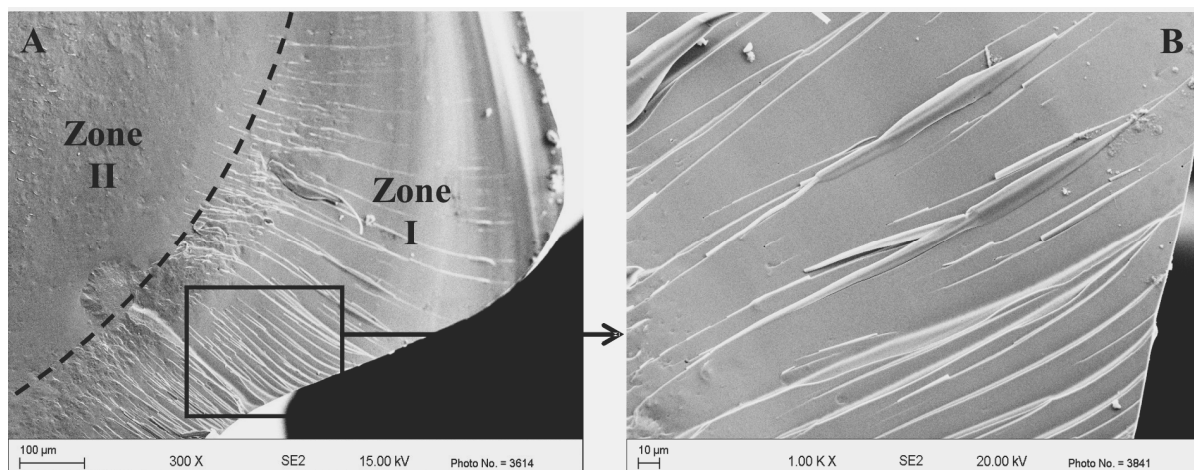
Fig. 35. SEM micrographs of the fracture morphology of $Fe_{72}B_{20}Si_4Nb_4$ amorphous rod in as-cast state with diameter of 2 mm: A – magn. 300x, B – magn. 1000x
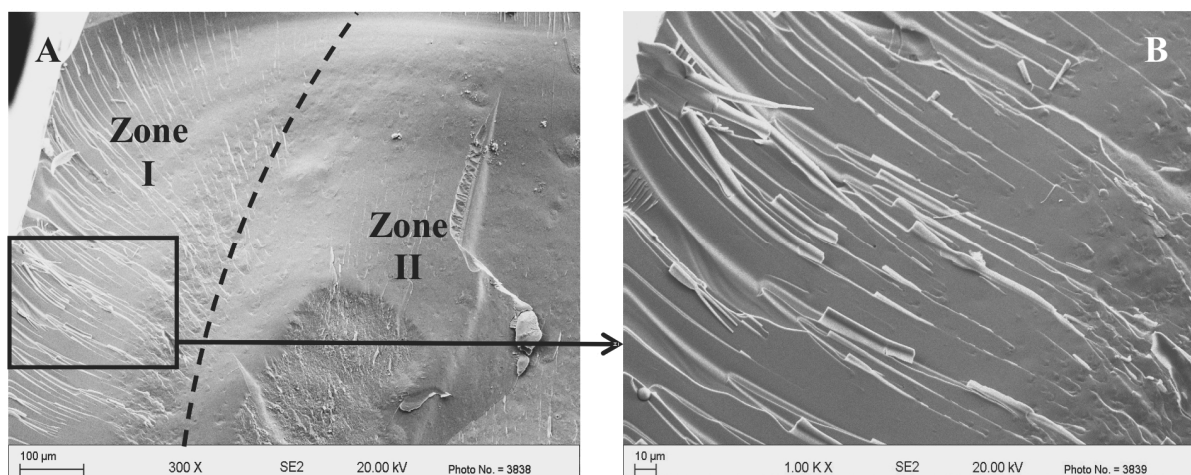
Fig. 36. SEM micrographs of the fracture morphology of $Fe_{72}B_{20}Si_4Nb_4$ amorphous rod in as-cast state with diameter of 2 mm: A – magn. 300x, B – magn. 1000x

The appearance of the fracture surface was investigated by SEM method at different magnifications for glassy rod samples. Figure 34 shows micrographs of as-cast glassy rod with diameter of 1.5 mm. What is more, Figures 35 and 36 present images of glassy rods with diameter of 2 mm, similarly.

The fracture surface appears to consist of small fracture zones, which leads to breaking of the samples into parts.

The presented fractures could be classified as mixed fractures with indicated two zones contain "vein" patterns (Zone I) and "smooth" areas (Zone II). The "vein" patterns (marked as Zone I) are characteristic for metallic glasses. The fracture surface of rod samples appears to consist of two different zones, which probably inform about different amorphous structures of the studied samples.
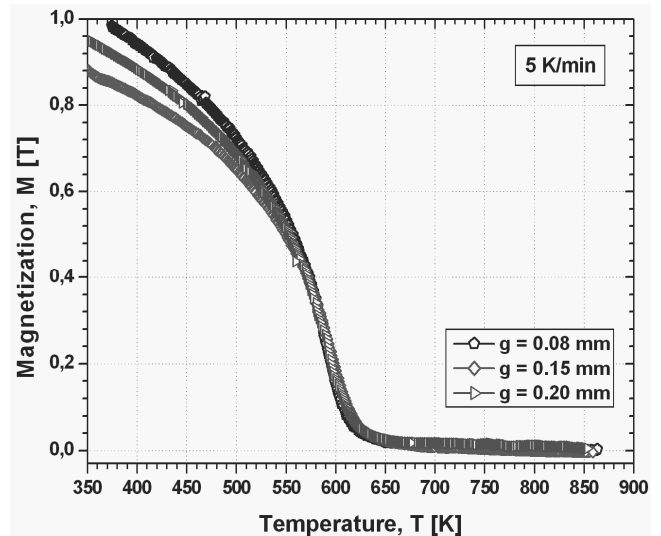
Fig. 37. Normalized curves of magnetization of $Fe_{72}B_{20}Si_4Nb_4$ glassy alloy in form of ribbons with thickness of 0.03, 0.05 and 0.06 mm in as-cast state

Fig. 39. Normalized curves of magnetization of $Fe_{72}B_{20}Si_4Nb_4$ glassy alloy in form of ribbons with thickness of 0.08, 0.15 and 0.20 mm in as-cast state

Fig. 38. dM/dT curves versus temperature of as-cast glassy $Fe_{72}B_{20}Si_4Nb_4$ alloy ribbons with thickness of 0.03, 0.05 and 0.06 mm in as-cast state
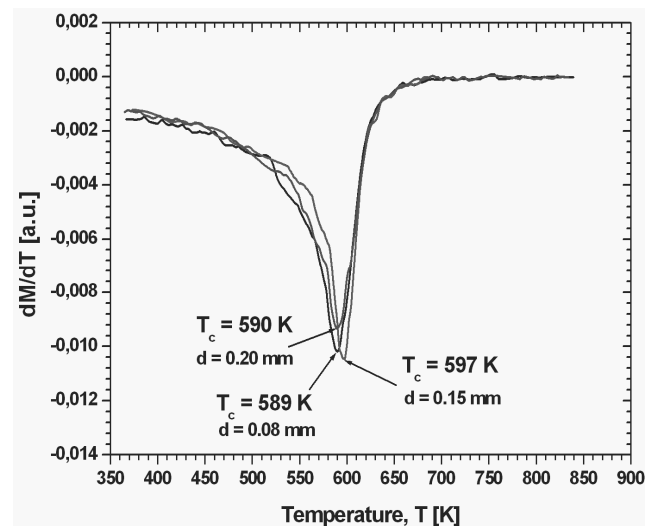
Fig. 40. dM/dT curves versus temperature of as-cast glassy $Fe_{72}B_{20}Si_4Nb_4$ alloy ribbons with thickness of 0.08, 0.15 and 0.20 mm in as-cast state

Figures 37 and 39 show normalized magnetization curves as a function of temperature with constant heating rate 5 K/min for glassy ribbons with thickness from 0.03 to 0.2 mm. The Curie temperature of amorphous phase of studied ribbons was determined from the dM/dT curves obtained of magnetization data (Figs. 38, 40).

The magnetization data informed that the Curie temperature (T_c) for ribbon with thickness from 0.03 to 0.06 mm increases with increasing of studied samples thickness.

For ribbon with thickness of 0.03 mm the Curie temperature reached a value of $T_c = 577$ K, for samples with thickness of 0.05 mm T_c has a value of 580 K and $T_c = 588$ for sample with thickness of 0.20 mm.

A stated variation of the Curie temperature is probably also due to changing of amorphous structure of studied material with sample thickness. The changing of the Curie temperatures could be noticed for further ribbons with thickness from 0.08 to 0.2 mm. For sample with thickness of 0.08 mm the Curie temperature has a value of 589 K, for ribbon with thickness of 0.15 mm the T_c increased to 597 K and for sample with thickness of 0.2 mm the Curie temperature reached of 590 K.

The Curie temperatures obtained from DSC curves for examined alloy cast in bulk form of rods and Curie temperature determined from normalized curves of magnetization are quite different because of different heating rtes used in both methods.

The initial magnetic permeability (μ_r) was determined for $Fe_{72}B_{20}Si_4Nb_4$ alloy for samples in form of ribbon and rod in as-cast state. The initial magnetic permeability is 1293 for ribbon with thickness of 0.03 mm, then μ_r has a higher value (1657) for ribbon with thickness of 0.08 mm and the ribbon with the highest thickness (g = 0.2 mm) has $\mu_r = 1083$.

The changing of (μ_r) obtained for samples with different thickness is another reason for non-homogenous of amorphous structure of tested metallic glasses.

Furthermore, the initial magnetic permeability of studied alloy in form of rods has a lower value and reached $\mu_r = 426$ for sample with diameter of 1.5 and $\mu_r = 161$ for rod with diameter of 2 mm.

Table 7 gives information about the Curie temperature and magnetic properties (initial magnetic permeability) of studied amorphous alloy in form of ribbons and rods.

Table 7.
The initial magnetic permeability and Curie temperature of $Fe_{72}B_{20}Si_4Nb_4$ bulk metallic glass in form of ribbons

Sample	Thickness [mm]	Magnetic properties	
		T_c [K]	μ_r
Ribbon	g = 0.03	577	1293
	g = 0.05	580	1786
	g = 0.06	588	1813
	g = 0.08	589	1657
	g = 0.15	597	1760
	g = 0.20	590	1083
Rod	ø = 1.5	567[*]	426
	ø = 2.0	570[*]	161

[*] results obtained from DSC investigations

In addition, Figures 41 and 42 present curves of maximum magnetic permeability obtained for glassy ribbon in as-cast state with thickness of 0.03 and 0.05 mm for comparison.

Fig. 41. Maximum magnetic permeability of $Fe_{72}B_{20}Si_4Nb_4$ glassy ribbon in as-cast state with thickness of 0.03 mm
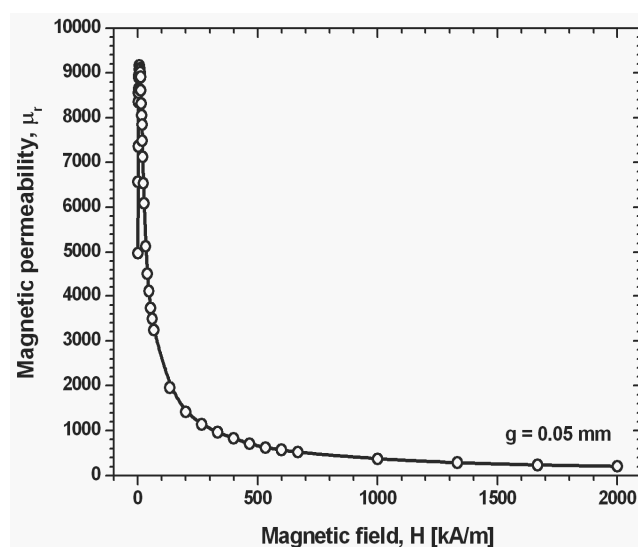
Fig. 42. Maximum magnetic permeability of $Fe_{72}B_{20}Si_4Nb_4$ glassy ribbon in as-cast state with thickness of 0.05 mm

The maximum magnetic permeability (μ_{rmax}) for glassy ribbon with thickness of 0.03 mm has a value of 6500, however the value of (μ_{rmax}) is much higher for sample with thickness of 0.05 mm and reached a value of 9100. This is a very good results, which allow to classify the studied Fe-based glassy alloy for suitable material for electric and magnetic applications.

From magnetic hysteresis loops obtained from VSM measurements of investigated materials - coercive force and magnetic saturation induction was determined. The magnetic hysteresis loops were achieved for ribbons with thickness from 0.03 to 0.06 mm presented in Figure 43 and for samples with thickness from 0.08 to 0.2 mm presented in Figure 44.

The coercive field (H_c) of tested metallic glasses has a value of 8.0 A/m for glassy ribbon with thickness of 0.03 mm, H_c = 4.8 A/m for ribbon with thickness of 0.08 mm and H_c = 5.6 A/m for sample with thickness of 0.20 mm. However, the coercive force for bulk glassy samples is much higher than for ribbon samples. H_c has a value of 40 A/m for rod with diameter of 1.5 mm and H_c = 65 A/m for rod with diameter of 2 mm.

Similarly, the saturation induction (B_s) of studied glassy ribbons has a value from 1.04 T for samples with the lowest thickness (g = 0.03 mm), then the B_s has a value of 1.12 T for ribbon with thickness of 0.08 mm and 1.10 T for ribbon with thickness of 0.20 mm, adequately. Furthermore, the magnetic saturation induction slightly decreases for glassy samples in form of rods. B_s for rods with diameter of 1.5 mm has a value of 1.13 T and 0.97 T for rod with diameter of 2 mm.

Table 8 gives information about the selected magnetic properties (magnetic saturation induction and coercive force) of studied amorphous alloy in form of ribbons and rods.

Table 8.
Magnetic properties of $Fe_{72}B_{20}Si_4Nb_4$ bulk metallic glass in form of ribbons obtained from magnetic hysteresis loops

Sample	Thickness [mm]	Magnetic properties	
		B_s [T]	H_c [A/m]
Ribbon	g = 0.03	1.04	8.0
	g = 0.05	1.05	5.6
	g = 0.06	1.06	7.2
	g = 0.08	1.12	4.8
	g = 0.15	1.04	5.6
	g = 0.20	1.10	5.6
Rod	ø = 1.5	1.13	39.8
	ø = 2.0	0.97	65.3

Some changes of H_c and B_s properties in function of sample thickness of studied glassy alloy confirmed the diversification of amorphous structure in as-cast state.
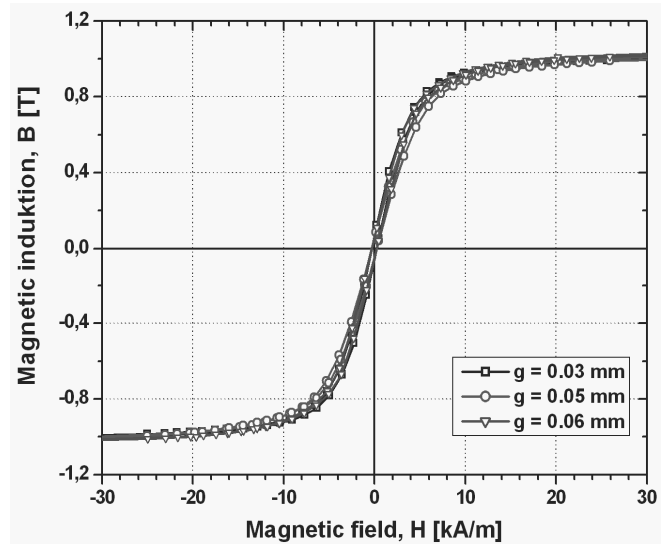
Fig. 43. Magnetic hysteresis loops of tested $Fe_{72}B_{20}Si_4Nb_4$ glassy alloy ribbons with thickness of 0.03, 0.05 and 0.06 mm
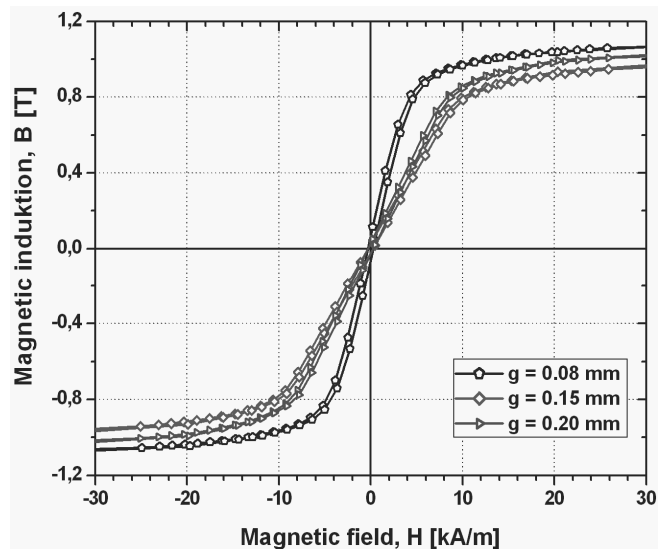
Fig. 44. Magnetic hysteresis loops of tested $Fe_{72}B_{20}Si_4Nb_4$ glassy alloy ribbons with thickness of 0.08, 0.15 and 0.20 mm

The initial magnetic permeability (μ_r) determined at room temperature versus annealing temperature (T_a) for ribbon and rod is shown in Fig. 45.

The initial magnetic permeability of examined alloy increases together with increasing of annealing temperature and reaches a distinct maximum at 773 K similarly for ribbon and rod samples. The temperature of annealing process, which corresponds to the maximum of initial magnetic permeability (μ_{rmax} = 2550 for ribbon, μ_{rmax} = 650 for rods) can be defined as the optimization annealing temperature (T_{op}).

However, distinct differences in the initial magnetic permeability between ribbons and rods could be explained by the different amorphous structure (higher cooling rates applied during the ribbons casting process).
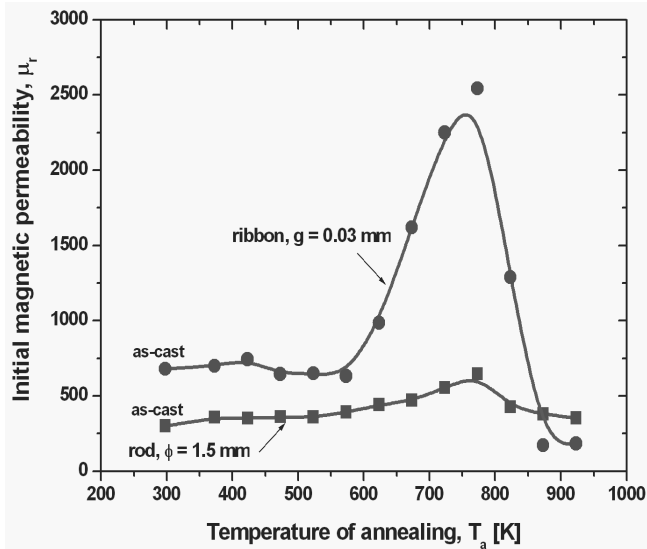
Fig. 45. Initial magnetic permeability of $Fe_{72}B_{20}Si_4Nb_4$ alloy determined at room temperature versus annealing temperature

Magnetic permeability relaxation (defined as magnetic after-effects) in function of annealing temperature for tested ribbon and rod samples is shown in Fig. 46. The intensity of $\Delta\mu/\mu$ is directly proportional to the concentration of defects in amorphous materials, i.e. free volume concentration [42-48]. The value of $\Delta\mu/\mu$ increases in the temperature range from 373 K to 473 K and from 373 K to 523 K for ribbons and rods, respectively.
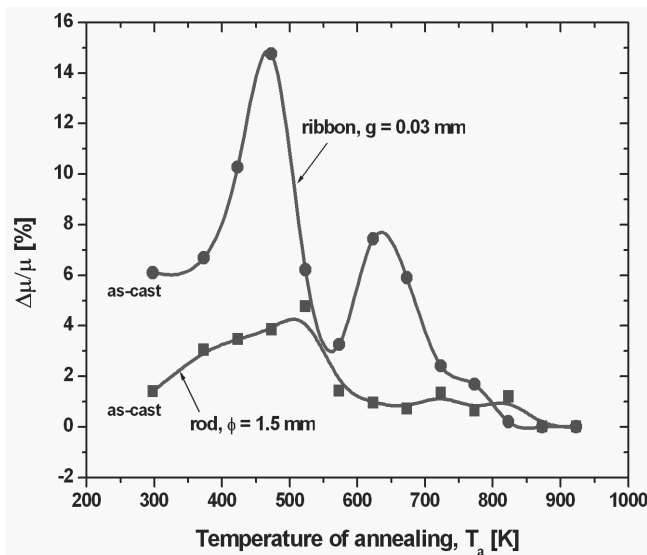
Fig. 46. Magnetic permeability relaxation of $Fe_{72}B_{20}Si_4Nb_4$ alloy determined at room temperature versus annealing temperature

Table 9.
Magnetic properties of studied $Fe_{72}B_{20}Si_4Nb_4$ alloy at optimization annealing temperature (T_{op})

Sample	T_{op} [K]	μ_r	$\Delta\mu/\mu$ [%]
Ribbon (g = 0.03 mm)	773	2550	1.7
Rod (ø = 1.5 mm)	773	650	0.6

The increase of annealing temperature causes the decrease of $\Delta\mu/\mu$ at temperatures higher than 523 K for rods and 623 K for ribbons. It is very important, because the optimization annealing temperature (T_{op}) corresponds to the decrease of magnetic instability ($\Delta\mu/\mu$). This effect means that the optimization annealing reduces time instabilities (free volume) of magnetic permeability.

Table 9 also gives information about magnetic properties of studied alloy in from of ribbon (g = 0.03 mm) and rod (ø = 1.5 mm) after optimization annealing temperature (T_{op}).

4. Conclusions

The investigations performed on the samples of $Fe_{72}B_{20}Si_4Nb_4$ as ribbon or rod shaped metallic glasses in as-cast state and after crystallization process allowed to formulate the following statements:

- the X-ray diffraction and transmission electron microscopy investigations revealed that the studied as-cast bulk metallic glasses (ribbons and rods) were amorphous,
- two stage crystallization process was observed for studied bulk amorphous alloy, the differences of crystallization temperature between ribbons and rods with chosen thickness are probably caused by different amorphous structures as a result of the different cooling rates in casting process,
- the SEM images showed that studied fractures could be classified as mixed fractures with indicated two zones contained "vein" and "smooth" areas,
- the magnetization data informed that the Curie temperature (T_c) for ribbon with thickness from 0.03 to 0.2 mm increases with increasing of studied samples thickness,
- the changing of chosen soft magnetic properties (μ_r, B_s, H_c) obtained for samples with different thickness is another result of non-homogenous of amorphous structure of tested metallic glasses,
- the maximum magnetic permeability (μ_{rmax}) for glassy ribbon with thickness of 0.05 mm reached a value of 9100, which allow to classify the studied Fe-based glassy alloy for suitable material for electric and magnetic applications,
- the annealing process in temperature range from 373 to 773 K causes structural relaxation of tested amorphous materials, which leads to changes in their physical properties,
- the qualitative phase analysis from X-ray and TEM diffraction data enables the identification of a single phase of α-Fe for sample annealed at 823 K; the precipitations for the ribbon annealed at 873 K corresponding to the temperature above the peak crystallization temperature of the first exothermic peak are a mixture of Fe_2B, Fe_3B and $Fe_{23}B_6$ and α-Fe phases;

- the initial magnetic permeability increased together with the increase of annealing temperature and reached a distinct maximum at 773 K for ribbons and rods,
- optimized annealing temperature (T_{op}) is connected with significant decrease of magnetic instability ($\Delta\mu/\mu$),
- the optimization effect (a real improvement of the initial magnetic permeability) takes place in amorphous phase of studied alloy.

Acknowledgements

References

[1] R. Zallen, Physics of amorphous materials, PWN, Warsaw, 1994 (in Polish).
[2] M. Soiński, Magnetic materials in engineering, COSiW SEP, Warsaw, 2001 (in Polish).
[3] H.K. Lachowicz, Amorphous magnetic materials: fabrication mathods, properties and technical applications, Proceedings of I Polish Seminar of Amorphous Magnetic Materials, Warsaw, 1983 (in Polish).
[4] R. Hasegawa, Glassy metals: magnetic, chemical and structural properties, CRC Press, Florida, 2000.
[5] J. Rasek, Some diffusion phenomena in crystalline and amorphous metals, Silesian University Press, Katowice, 2000 (in Polish).
[6] K. Szaciłowski, Chosen aspects of nanotechnology. Classification and properties of nanomaterials, Foundry – Science and Practice 3 (2004) 3-16 (in Polish).
[7] A. Inoue, K. Hashimoto, Amorphous and nanocrystalline materials: preparation, properties and applications, Springer, 2001.
[8] A. Inoue, A. Makino, T. Mizushima, Ferromagnetic bulk glassy alloys, Journal of Magnetism and Magnetic Materials 215-216 (2000) 246-252.
[9] H. S. Chen, Metallic Glasses, Chinese Journal of Physics 28 (1990) 407-425.
[10] K. Urban, C.M. Schneider, T. Brückel, S. Blügel, K. Tillmann, W. Schweika, M. Lentzen, L. Baumgarten, Probing the Nanoworld, Microscopies, Scattering and Spectroscopies of the Solid State, Lecture Manuscripts of the 38th Spring School 2007.
[11] Z.P. Lu, X. Hu, Y. Li, S.C. Ng, Glass forming ability of La-Al-Ni-Cu and Pd-Si-Cu bulk metallic glasses, Materials Science and Engineering A304–306 (2001) 679-682.
[12] L. Liu, K.C. Chan, G.K.H. Pang, High-resolution TEM study of the microstructure of $Zr_{65}Ni_{10}Cu_{7.5}Al_{7.5}Ag_{10}$ bulk metallic glass, Journal of Crystal Growth 265 (2004) 642-649.
[13] Y. Zhang, Y.F. Ji, D.Q. Zhao, Y.X. Zhuang, R.J. Wang, M.X. Pan, Y.D. Dong, W.H. Wang, Glass forming ability and properties of Zr/Nb-based bulk metallic glasses, Scripta Materialia 44 (2001) 1107-1112.
[14] Z. Bian, G.L. Chen, G. He, X.D. Hui, Microstructure and ductile-brittle transition of as-cast Zr-based bulk glass alloys under compressive testing, Materials Science and Engineering A316 (2001) 135-144.
[15] L. Liu, C.L. Qiu, H. Zou, K.C. Chan, The effect of the microalloying of Hf on the corrosion behavior of Zr-Cu-Ni-Al bulk metallic glass, Journal of Alloys and Compounds 399 (2005) 144-148.
[16] W. Chen, Y. Wang, J. Qiang, C. Dong, Bulk metallic glasses in the Zr-Al-Ni-Cu system, Acta Materialia 51 (2003) 1899-1907.
[17] F.M. Alamgir, H. Jain, R.B. Schwarz, O. Jin, D.B. Williams, Electronic structure of Pd-based bulk metallic glasses, Journal of Non-Crystalline Solids 274 (2000) 289-293.
[18] V.V. Molokanov, M.I. Petrzhik, T.N. Mikhailova, T.A. Sviridova, N.P. Djakonova, Formation of bulk (Zr, Ti)-based metallic glasses, Journal of Non-Crystalline Solids 250-252 (1999) 560-565.
[19] T. Itoi, T. Takamizawa, Y. Kawamura, A. Inoue, Fabrication of $Co_{40}Fe_{22}Nb_8B_{30}$ bulk metallic glasses by consolidation of gas-atomized powders and their soft magnetic properties, Scripta Materialia 45 (2001) 1131-1137.
[20] D. Xu, G. Duan, W.L. Johnson, C. Garland, Formation and properties of new Ni-based amorphous alloys with critical casting thickness up to 5 mm, Acta Materialia 52 (2004) 3493-3497.
[21] Q. Li, Formation of ferromagnetic bulk amorphous $Fe_{40}Ni_{40}P_{14}B_6$ alloys, Materials Letters 60 (2006) 3113-3117.
[22] M. Shapaan, J. Lábár, J. Lendvai, L.K. Varga, Crystallization behavior of $Fe_{62}Nb_{8-x}Zr_xB_{30}$ bulk amorphous alloy, Materials Science and Engineering A 375-377 (2004) 789-793.
[23] Q.J. Chen, H.B. Fan, L. Ye, S. Ringer, J.F. Sun, J. Shen, D.G. McCartney, Enhanced glass forming ability of Fe-Co-Zr-Mo-W-B alloys with Ni addition, Materials Science and Engineering A 402 (2005) 188-192.
[24] J. Basu, S. Ranganathan, Bulk metallic glasses: A new class of engineering materials, Sadhana 28 (2003) 783-798.
[25] A. Inoue, High strength bulk amorphous alloys with low critical cooling rates, Materials Transactions JIM 36 (1995) 866-875.
[26] A. Inoue, Bulk amorphous and nanocrystalline alloys with high functional properties, Materials Science and Engineering A304-306 (2001) 1-10.
[27] A. Inoue, B.L. Shen, C.T. Chang, Fe- and Co-based bulk glassy alloys with ultrahigh strength of over 4000 MPa, Intermetallics 14 (2006) 936-944.
[28] W.H. Wang, C. Dong, C.H. Shek, Bulk metallic glasses, Materials Science and Engineering R 44 (2004) 45-89.
[29] A. Inoue, Bulk amorphous and nanocrystalline alloys with high functional properties, Materials Science and Engineering A304-306 (2001) 1-10.
[30] A. Inoue, B.L. Shen, C.T. Chang, Fe- and Co-based bulk glassy alloys with ultrahigh strength of over 4000 MPa, Intermetallics 14 (2006) 936-944.
[31] W.H. Wang, C. Dong, C.H. Shek, Bulk metallic glasses, Materials Science and Engineering R 44 (2004) 45-89.

[32] Z.P. Lu, C.T. Liu, A new glass-forming ability criterion for bulk metallic glasses, Acta Materialia 50 (2002) 3501-3512.

[33] Y. Li, S.C. Ng, C.K. Ong, H.H. Hng, T.T. Goh, Glass forming ability of bulk glass forming alloys, Scripta Materialia 36 (1997) 783-787.

[34] G.J. Fan, H. Choo, P.K. Liaw, A new criterion for the glass-forming ability of liquids, Journal of Non-Crystalline Solids 353 (2007) 102-107.

[35] A. Hruby, Evaluation of glass-forming tendency by means of DTA, Czechoslovak Journal of Physics B22 (1972) 1187-1193.

[36] M. Saad, M. Poulain, Glass forming ability criterion, Materials Science Forum 19-20 (1987) 11-18.

[37] B. Lemley, Glassy Metals. Harder, stronger and better - the material of the future, Discover 25/4 (2004).

[38] T. Kulik, Nanocrystallization of metallic glasses, Journal of Non-Crystalline Solids 287 (2001) 145-161.

[39] W. H. Wang, Crystallization of ZrTiCuNiBe bulk metallic glasses, Annales de Chimie Science des Materiaux 27/5 (2002) 99-105.

[40] H. Kronmüller, Micromagnetism and microstructure of amorphous alloys, Journal of Applied Physics 52/3 (1981) 1859-1864.

[41] H. Kronmüller, Magnetization process and the microstructure in amorphous metals, Journal de Physique 41 (1980) 518-625.

[42] P. Kwapuliński, J. Rasek, Z. Stokłosa, G. Haneczok, M. Gigla, Structural relaxation and crystallisation processes in $FeCu_1XSi_{13}B_9$ (X = Mo, Cr, Zr) amorphous alloys, Journal of Magnetism and Magnetic Materials 215-216 (2000) 334-336.

[43] Z. Stokłosa, P. Kwapuliński, G. Haneczok, J. Rasek, Structural relaxation and formation of nanocrystalline phase in Fe-X-Si-B amorphous alloys, Journal of Physics IV France 8 (1998) 51-54.

[44] P. Kwapuliński, J. Rasek, Z. Stokłosa, G. Haneczok, Optimization of soft magnetic properties in $Fe-Cu-X-Si_{13}B_9$ (X = Cr, Mo, Zr) amorphous alloys, Journal of Magnetism and Magnetic Materials 234 (2001) 218-226.

[45] Z. Stokłosa, J. Rasek, P. Kwapuliński, G. Haneczok, G. Badura, J. Lelątko, Nanocrystallisation of amorphous alloys based on iron, Materials Science and Engineering C 23 (2003) 49-53.

[46] Z. Stokłosa, G. Badura, P. Kwapuliński, J. Rasek, G. Haneczok, J. Lelątko, L. Pająk, Influence of alloying additions on enhancement of soft magnetic properties effect and crystallisation in FeXSiB (X = Cu, V, Co, Zr, Nb) amorphous alloys, Solid State Phenomena 130 (2007) 171-174.

[47] P. Kwapuliński, J. Rasek, Z. Stokłosa, G. Haneczok, Magnetic properties of amorphous and nanocrystalline alloys based on iron, Journal of Materials Processing Technology 157-158 (2004) 735-742.

[48] P. Kwapuliński, J. Rasek, Z. Stokłosa, G. Badura, B. Kostrubiec, G. Haneczok, Magnetic and mechanical properties in FeXSiB (X=Cu, Zr, Co) amorphous alloys, Archives of Materials Science and Engineering 31\1 2008 25-28.

[49] A. Inoue, A. Takeuchi, Recent progress in bulk glassy alloys, Materials Transactions JIM 43 (2002) 1892-1906.

[50] M.R. Surowiec, Quasicrystals, WNT, Warsaw, 2008 (in Polish).

[51] R.W. Cahn, P. Haasen, E.J. Kramer, Materials Science and Technology: structure of solids, VCH Press, Weiheim-New York-Basel-Cambridge, 1993.

[52] A. Inoue, B.L. Shen, C.T. Chang, Super-high strength of over 4000 MPa for Fe-based bulk glassy alloys in $[(Fe_{1-x}Co_x)_{0.75}B_{0.2}Si_{0.05}]_{96}Nb_4$ system, Acta Materialia 52 (2004) 4093-4099.

[53] B. Shen, C. Chang, A. Inoue, Formation, ductile deformation behavior and soft-magnetic properties of (Fe,Co,Ni)-B-Si-Nb bulk glassy alloys, Intermetallics 15 (2007) 9-16.

[54] A. Inoue, B. Shen, A. Takeuchi, Fabrication, properties and applications of bulk glassy alloys in late transition metal-based systems, Materials Science and Engineering A 441 (2006) 18-25.

[55] Ch. Chang, B. Shen, A. Inoue, Synthesis of bulk glassy alloys in the (Fe,Co,Ni)-B-Si-Nb system, Materials Science and Engineering A 449-451 (2007) 239-242.

[56] R. Nowosielski, R. Babilas, S. Griner, G. Dercz, A. Hanc, Crystallization of $Fe_{72}B_{20}Si_4Nb_4$ metallic glasses ribbons, Journal of Achievements in Materials and Manufacturing Engineering 34/1 (2009) 15-22.

[57] D. Szewieczek, J. Tyrlik-Held, S. Lesz, Structure and mechanical properties of amorphous $Fe_{84}Nb_7B_9$ alloy during crystallization, Journal of Achievements in Materials and Manufacturing Engineering 24 (2007) 87-90.

[58] D. Szewieczek, T. Raszka, J. Olszewski, Optimisation the magnetic properties of the $(Fe_{1-x}Co_x)_{73.5}Cu_1Nb_3Si_{13.5}B_9$ (x=10; 30; 40) alloys, Journal of Achievements in Materials and Manufacturing Engineering 20 (2007) 31-36.

[59] S. Lesz, D. Szewieczek, J.E. Frąckowiak, Structure and magnetic properties of amorphous and nanocrystalline $Fe_{85.4}Hf_{1.4}B_{13.2}$ alloy, Journal of Achievements in Materials and Manufacturing Engineering 19 (2006) 29-34.

[60] S. Lesz, D. Szewieczek, J. Tyrlik-Held, Correlation between fracture morphology and mechanical properties of NANOPERM alloys, Archives of Materials Science and Engineering 29/2 (2008) 73-80.

[61] T. Haga, K. Inoue, H. Watari, Micro-forming of Al-Si foil, Journal of Achievements in Materials and Manufacturing Engineering 40/2 (2010) 115-122.

[62] R. Nowosielski, R. Babilas, Structure and magnetic properties of $Fe_{36}Co_{36}B_{19}Si_5Nb_4$ bulk metallic glasses, Journal of Achievements in Materials and Manufacturing Engineering 30/2 (2008) 135-140.

[63] R. Nowosielski, R. Babilas, S. Griner, Z. Stokłosa, Structure and soft magnetic properties of $Fe_{72}B_{20}Si_4Nb_4$ bulk metallic glasses, Archives of Materials Science and Engineering 35/1 (2009) 13-20.

[64] R. Nowosielski, R. Babilas, Structure and properties of selected Fe-based metallic glasses, Journal of Achievements in Materials and Manufacturing Engineering 37/2 (2009) 332-339.

[65] R. Nowosielski, R. Babilas, S. Griner, T. Czeppe, Structure, thermal and magnetic properties of $Fe_{43}Co_{14}Ni_{14}B_{20}Si_5Nb_4$ bulk metallic glass, Journal of Achievements in Materials and Manufacturing Engineering 38/2 (2010) 123-130.

[66] R. Nowosielski, R. Babilas, Preparation, structure and properties of Fe-based bulk metallic glasses, Journal of Achievements in Materials and Manufacturing Engineering, 40/2 (2010) 123-130.

[67] J. Wrona, M. Czapkiewicz, T. Stobiecki, Magnetometer for the measurements of the hysteresis loop of ultrathin magnetic layers, Journal of Magnetism and Magnetic Materials 196 (1999) 935-936.

[68] J. Wrona, T. Stobiecki, M. Czapkiewicz, R. Rak, T. Ślęzak, J. Korecki, C.G. Kim, R-VSM and MOKE magnetometers for nanostructures, Journal of Magnetism and Magnetic Materials 272-276 (2004) 2294-2295.